Journal of Theoretical Biology 253 (2008) 638–658

Contents lists available at ScienceDirect

Journal of Theoretical Biology

journal homepage: www.elsevier.com/locate/yjtbi

Modelling of stomatal density response to atmospheric CO_2

W. Konrad *, A. Roth-Nebelsick, M. Grein

Institute for Geosciences, University of Tübingen, Sigwartstrasse 10, D-72076 Tübingen, Germany

ARTICLE INFO

Article history:
Received 2 August 2007
Received in revised form
11 March 2008
Accepted 27 March 2008
Available online 6 April 2008

Keywords:
Palaeoclimate
Gas exchange
Fossil plants
Stomatal conductance
Photosynthesis

ABSTRACT

Stomatal density tends to vary inversely with changes in atmospheric CO_2 concentration (C_a). This phenomenon is of significance due to: (i) the current anthropogenic rise in C_a and its impact on vegetation, and (ii) the potential applicability for reconstructing palaeoatmospheric C_a by using fossil plant remains. It is generally assumed that the inverse change of stomatal density with C_a represents an adaptation of epidermal gas conductance to varying C_a. Reconstruction of fossil C_a by using stomatal density is usually based on empirical curves which are obtained by greenhouse experiments or the study of herbarium material. In this contribution, a model describing the stomatal density response to changes in C_a is introduced. It is based on the diffusion of water vapour and CO_2, photosynthesis and an optimisation principle concerning gas exchange and water availability. The model considers both aspects of stomatal conductance: degree of stomatal aperture and stomatal density. It is shown that stomatal aperture and stomatal density response can be separated with stomatal aperture representing a short-term response and stomatal density a long-term response. The model also demonstrates how the stomatal density response to C_a is modulated by environmental factors. This in turn implies that reliable reconstructions of ancient C_a require additional information concerning temperature and humidity of the considered sites. Finally, a sensitivity analysis was carried out for the relationship between stomatal density and C_a in order to identify critical parameters (= small parameter changes lead to significant changes of the results). Stomatal pore geometry (pore size and depth) represents a critical parameter. In palaeoclimatic studies, pore geometry should therefore also be considered.

1. Introduction

Numerous studies have shown that stomatal densities vary inversely with changing atmospheric CO_2 (termed as C_a throughout the rest of this text). This has been demonstrated by observations on herbarium material (Woodward, 1987; Penuelas and Matamala, 1990; van de Water et al., 1994; Beerling and Kelly, 1997; Kouwenberg et al., 2003; Garcia-Amorena et al., 2006), greenhouse experiments (Woodward and Bazzazz, 1988; Kürschner et al., 1998; Royer et al., 2001; Teng et al., 2006) and palaeobotanical studies (Kürschner, 1996; Royer, 2001; Beerling and Royer, 2002; McElwain et al., 2002). Since stomata represent the gateways for gas exchange and are therefore involved in a plant's reaction to rising C_a level, stomatal responses to C_a are of general interest (Tricker et al., 2005). Furthermore, C_a-induced changes of stomatal density appear to represent a valuable proxy for palaeoatmospheric C_a. In various studies, stomatal density was used for reconstructing ancient C_a (Kürschner et al., 1996; Royer et al., 2001; Beerling, 2002; McElwain et al., 2002; Kürschner et al., 2008).

It is assumed that the reason for the $v(C_a)$-response is due to the adaptation of the epidermal permeability which is dependent on stomatal density and stomatal architecture (i.e. pore area and pore depth) to changing C_a-level (Woodward, 1987). This is reasonable since an increase in C_a increases the diffusional CO_2 flux into the leaf under a given stomatal conductance and CO_2 gradient. Perception of the C_a-signal was shown for *Arabidopsis thaliana* to occur in mature leaves, with the HIC gene being involved (Lake et al., 2001, 2002). If C_a increases, a plant can decrease its stomatal density while maintaining the required CO_2 influx. This is advantageous since stomata represent sites of water loss and construction expenses can be saved. It is therefore to be expected that adaptations of stomatal density to C_a are of selective value for a plant lineage. The current technique for reconstructing past CO_2 is based on empirically established transfer functions. The stomatal density (termed v in the following) of extant material grown under different C_a concentrations—herbarium material or potted plants grown in greenhouses—is obtained and a function is fitted to the data points (Beerling and Royer, 2002). Since the $v(C_a)$-response is species specific, a transfer function has to be established for each

* Corresponding author. Tel.: +49 7071 2973561.
E-mail addresses: wilfried.konrad@uni-tuebingen.de (W. Konrad), anita.roth@uni-tuebingen.de (A. Roth-Nebelsick), michaela.grein@t-online.de (M. Grein).

0022-5193/$ - see front matter © 2008 Elsevier Ltd. All rights reserved.
doi:10.1016/j.jtbi.2008.03.032

considered species. v is influenced by various environmental factors (temperature, humidity), the stomatal index (the number of stomata in relation to the number of epidermis cells) is therefore often applied as a surrogate parameter which shows less variation (Beerling et al., 1998; Poole and Kürschner, 1999).

There are, however, also reports about unchanging stomatal frequency under increasing C_a. For example, in two studies which were performed within the framework of FACE (free-air enrichment) experiments, no stable and/or significant decreases of stomatal density under elevated C_a could be observed (Reid et al., 2003; Tricker et al., 2005). On some occasions, stomatal density is even reported to increase with elevated C_a (Lawson et al., 2002). Since a decrease in stomatal conductance due to decreasing stomatal aperture under elevated CO_2 is almost always observed in experiments (Medlyn et al., 2001; Ainsworth and Long, 2005), it was suggested by the authors that C_a-induced changes of stomatal density require an evolutionary process (Reid et al., 2003; Tricker et al., 2005). This is consistent with results of a literature survey which indicate that the frequency of taxa which show an inverse change of stomatal density with C_a increases with increasing age of the material (fossil > subfossil > Herbarium > Recent material) (Royer, 2001). The empirical method of producing transfer functions makes no use of the assumed underlying biological mechanism of adaptation of the total epidermal conductance to C_a. An approach was devised by Wynn (2003) who applied the process of gas diffusion through the epidermis (and thus through the stomata) as basis for the curve fitting which is completed by obtaining empirical parameters from measured data.

In order to fully explore the $v(C_a)$-responses it is indispensable to consider the process of photosynthesis since both transpiration and assimilation are affected by stomatal conductance and therefore by stomatal density. A mechanistic model of the $v(C_a)$-response would be desirable, because: (i) ecophysiological aspects of the $v(C_a)$-response could be explored, (ii) the tacitly assumed evolutionary optimisation process of the response in the case of fossil material could be described (the current $v(C_a)$-response data represent phenotypic reactions and it is not clear whether they are valid for responses on the evolutionary level) and (iii) sensitivity analyses would be possible which provide insight into the reliability of the approach, identify critical parameters and supply a meaningful error margin. In this contribution, it will be attempted to model the $v(C_a)$-response by coupling diffusion and photosynthesis. The approach is completed by including an optimisation principle which introduces an interrelationship between gas exchange and the availability of water. Finally, the model will be applied to *Ginkgo biloba*. This species was used repeatedly for reconstructing ancient C_a levels and various data sets are therefore available (Sun et al., 2003; Royer et al., 2001).

2. The model

2.1. Diffusion of water vapour and carbon dioxide

The movement of water vapour and carbon dioxide into and out of plants is governed by the process of diffusion, described by Fick's first law:

$$\mathbf{j} = -S \operatorname{grad} c \tag{1}$$

In the following, c stands either for the concentration w of water vapour or the concentration C of carbon dioxide. The Diffusion equation (also known as Fick's second law) is derived from applying the principle of mass conservation to Fick's first law. It reads as

$$\Sigma = \frac{\partial c}{\partial t} + \operatorname{div}(S \operatorname{grad} c) \tag{2}$$

If the source (or sink) term $\Sigma = \Sigma(x, y, z, t, c)$ is independent of c and if the effective conductance $S = S(x, y, z)$ and appropriate boundary conditions for c are prescribed, the diffusion Eq. (2) has exactly one solution for the concentration $c = c(x, y, z, t)$ of water vapour or carbon dioxide. Once $c = c(x, y, z, t)$ is calculated the flux $\mathbf{j}(x, y, z, t)$ follows from (1).

It is impossible to solve (2) in all generality for realistic conditions, because the complex network of voids and channels which form the intercellular air space implies very complex boundary conditions for (2). If, however, we claim that c and $\mathbf{j}$ shall be correct only down to dimensions of a few diameters of a typical cell, we can employ approximations which lead to symmetries that allow for drastic simplifications in (2) and (1). In that case, we can apply (i) the porous medium approach and assume that (ii) the effective conductance S remains constant within the functionally different tissue layers of a plant leaf. We may furthermore assume (iii) stationary conditions. These approximations are discussed in Appendix A.1.

After applying the various approximations, the differential equation (2) simplifies to

$$\Sigma = S\left(\frac{\partial^2 c}{\partial x^2} + \frac{\partial^2 c}{\partial y^2} + \frac{\partial^2 c}{\partial z^2}\right) \tag{3}$$

The source (or sink) term Σ (if present) and the concentration c are functions of the coordinates (x, y, z). Leaves are flat objects whose lateral dimensions (several centimeters) are about a factor 10^4 greater than stomatal radii (a few micrometers). This implies, together with the layered structure of leaves:

(i) The general direction of the diffusional flux is perpendicular to the leaf plane, i.e. parallel to the x-axis, if we orient the coordinate system such that the y- and z-axes are parallel to the leaf plane.
(ii) In the coordinate system defined in (i) all quantities appearing in Eqs. (3) and (1) depend only on the coordinate x, but not on y or z.

Then the three-dimensional partial differential equation (3) reduces to a one-dimensional ordinary differential equation for $c(x)$

$$\Sigma(x) = S\frac{\mathrm{d}^2 c(x)}{\mathrm{d}x^2} \tag{4}$$

which has to be solved separately for each layer involved in gas diffusion: assimilation layer (*as*), stomatal layer (*sl*) and boundary layer (*bl*). Fick's first law (1) simplifies then to

$$j(x) = -S\frac{\mathrm{d}c}{\mathrm{d}x}(x) \tag{5}$$

where the flux j is directed parallel to the x-axis.

2.2. Sources and sinks

Within boundary layer and stomatal layer we may assume $\Sigma(x) = 0$, both for CO_2- and H_2O-molecules. With respect to sources and sinks within the assimilation layer, the following simplification was applied. The plane which is located near the upper boundary of the assimilation layer and parallel to the leaf surface (the broken line, denoted c_i in Fig. 1) serves as (idealised) source of water vapour and as sink for carbon dioxide molecules. Within the assimilation layer (as depicted in Fig. 1) holds $\Sigma(x) = 0$.

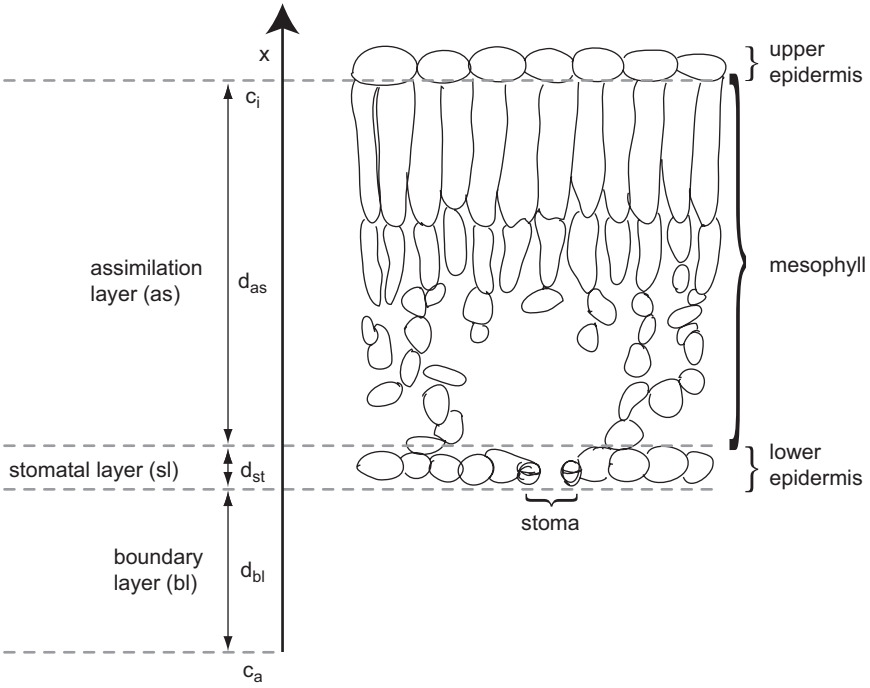

Fig. 1. Schematic cross section through a leaf (based on a drawing by Birgit Binder, Tübingen). The picture shows the different layers of a typical angiosperm leaf and their representation within the model. The assimilation layer (*as*) represents the mesophyll and the stomatal layer (*sl*) includes epidermis and stomata. The boundary layer (*bl*) located at the (lower) leaf surface is also considered in the model. c_a denotes either the atmospheric CO_2 concentration C_a or the atmospheric humidity w_a. c_i refers to C_i and w_i, the internal CO_2 and H_2O concentrations. d_{as}, d_{st} and d_{bl}: thickness of assimilation layer, stomatal layer and boundary layer, respectively.

In this case Eq. (4) becomes *very* simple

$$0 = S\frac{\mathrm{d}^2 c}{\mathrm{d}x^2}(x) \tag{6}$$

with the readily obtained solutions

$$c_{as}(x) = a_{as}x + b_{as} \quad c_{st}(x) = a_{st}x + b_{st} \quad c_{bl}(x) = a_{bl}x + b_{bl} \tag{7}$$

and, from Eq. (5),

$$j_{as}(x) = -S_{as}a_{as} \quad j_{st}(x) = -S_{st}\,a_{st} \quad j_{bl}(x) = -S_{bl}\,a_{bl} \tag{8}$$

where it is understood that positive fluxes j_k ($k = as, sl, bl$) flow parallel, negative fluxes antiparallel to the x-axis (c.f. Fig. 1). The a_k and b_k are arbitrary constants. Their values are calculated from requiring: (i) that the c_k and j_k (from Eqs. (7) and (8)) are continuous at the planes separating adjacent boundary layers, and, (ii) that c_{bl} and c_{as} attain the values c_a and c_i, respectively, at the lower and upper boundary of the region depicted in Fig. 1.

The effective conductances S_k differ from layer to layer. They are defined in analogy to (A.2) as

$$S_{as} := D\frac{n_{as}}{\tau_{as}^2} \tag{9}$$

and similar expressions for (*sl*) and (*bl*). D denotes either D_{H_2O} or D_{CO_2}.

Applying the continuity conditions we find: (i) that the flux does *not* depend explicitly on x, and, (ii) that $j_{as} = j_{st} = j_{bl} =: j$. It is given as

$$j = \frac{D(c_i - c_a)}{\left(\dfrac{d_{bl}\tau_{bl}^2}{n_{bl}} + \dfrac{d_{st}\tau_{st}^2}{n_{st}} + \dfrac{d_{as}\tau_{as}^2}{n_{as}}\right)} \tag{10}$$

The quantities in (10) can be specified more explicitly (c.f. Fig. 1):

- *Boundary layer*: Obviously, porosity and tortuosity attain the very simple values

$$n_{bl} = 1 \quad \text{and} \quad \tau_{bl} = 1 \tag{11}$$

d_{bl} depends (see Nobel, 1999) on the wind velocity u_{wind} and a typical leaf length l according to the empirical formula (m and s denote the units meter and second, respectively)

$$d_{bl} = 4 \times 10^{-3}\ \frac{m}{\sqrt{s}}\sqrt{\frac{l}{u_{wind}}} \tag{12}$$

- *Stomatal layer*: The porosity of the stomatal layer can be expressed in terms of the cross-sectional area of a stoma a_{st} and the stomatal density v as

$$n_{st} = a_{st}v \tag{13}$$

Since the stomatal channels are straight openings we find for their tortuosity

$$\tau_{st} = 1 \tag{14}$$

d_{st} is a combination of the geometrical thickness d_{st}^{geom} and a correction $\sqrt{a_{st}/\pi}$ which is due to the fact that the surfaces of constant CO_2 and H_2O concentration bulge out from the stomata into boundary layer and intercellular airspace (see Nobel, 1999). Thus,

$$d_{st} = d_{st}^{geom} + \sqrt{a_{st}/\pi} \tag{15}$$

In the following, the model will be developed by using v and not the stomatal index which is preferred in most empirical approaches. The reason for this is simply that v has a direct relationship to gas exchange and not the stomatal index.

- *Assimilation layer*: Values for porosity, tortuosity and thickness of the layer should be obtained by measurements from specimen. Typical values are of the order of $n_{as} \approx 0.35$, $\tau_{as} \approx 1.571$ and $d_{as} \approx 200\,\mu\mathrm{m}$.

Insertion of expressions (11), (13) and (14) into Eq. (10) results in a somewhat simplified, intermediate version of (10)

$$j = \frac{va_{st}D(c_a - c_i)}{\left[d_{bl} + d_{as}\frac{\tau_{as}^2}{n_{as}}\right]va_{st} + d_{st}} \tag{16}$$

Writing down expression (16) separately for water vapour ($c_i = w_i$, $c_a = w_a$ and $D = D_{H_2O}$) and carbon dioxide ($c_i = C_i$, $c_a = C_a$ and $D = D_{CO_2}$) results in

$$j_{H_2O} = \frac{va_{st}\,D_{H_2O}}{\left[d_{bl} + d_{as}\frac{\tau_{as}^2}{n_{as}}\right]va_{st} + d_{st}} \times (w_a - w_i) \tag{17}$$

and

$$j_{CO_2} = \frac{va_{st}D_{CO_2}}{\left[d_{bl} + d_{as}\frac{\tau_{as}^2}{n_{as}}\right]va_{st} + d_{st}} \times (C_a - C_i) \tag{18}$$

where d_{bl} and d_{st} are as given in (12) and (15), respectively. To keep notation simple we define the first factor on the right-hand side of (18) as the total conductance with respect to CO_2

$$g = \frac{va_{st}D_{CO_2}}{\left[d_{bl} + d_{as}\frac{\tau_{as}^2}{n_{as}}\right]va_{st} + d_{st}} \tag{19}$$

Employing the definition $a := D_{H_2O}/D_{CO_2}$ the total conductance with respect to H_2O (i.e. the first factor on the right-hand side of (17)) becomes ag.

Since we restrict our model to stationary conditions all carbon dioxide molecules entering the plant become eventually assimilated, hence $j_{CO_2} = A$ where A denotes the assimilation rate. Eq. (18) can now be rewritten in the more compact form

$$A = g(C_a - C_i) \tag{20}$$

Stationary conditions imply also $-j_{H_2O} = E$, with E representing the transpiration rate. The minus sign in front of j_{H_2O} ensures that E attains positive values. Because w_i is defined as the water vapour concentration around the transpiring mesophyll cells it equals w_{sat}, the saturation value of water vapour concentration in air (equivalent to 100% relative humidity). This depends on temperature T (see Appendix B.3). Inserting expression (19), $a = D_{H_2O}/D_{CO_2}$ and the equality $w_i = w_{sat}$ into (17) we find

$$E = ag(w_{sat} - w_a) \tag{21}$$

In contrast to (21), expression (20) represents only an intermediate result: it relates—in analogy to (21)—A to C_i. C_i, however, does not attain a fixed value as is the case with w_{sat}. It is rather coupled to A by a second relation expressing the intensity of photosynthesis. In other words, C_i has to be known in order to calculate A (Katul et al., 2000). This will be further discussed in the following section.

2.3. Coupling of diffusion and assimilation model

We use the Farquhar model of assimilation (see Farquhar et al., 1980, 2001):

$$A = \left(1 - \frac{\Gamma}{C_i}\right)\min\{W_c, W_j\} - R_d \tag{22}$$

with

$$W_c := V_{max}\frac{C_i}{C_i + K_c\left(1 + \frac{p_o}{K_o}\right)}$$

$$W_j := \left(\frac{2}{9}J\right)\frac{C_i}{C_i + \frac{7}{3}\Gamma}$$

where

$$J := \frac{Q_2 + J_{max} - \sqrt{(Q_2 + J_{max})^2 - 4\Theta_{PSII}Q_2J_{max}}}{2\Theta_{PSII}}$$

and

$$Q_2 := Q\alpha_l\Phi_{PSII,max}\beta \tag{23}$$

The expression $\min\{W_c, W_j\}$ denotes the smaller of W_c and W_j for given values of C_i and J. The variables used in (22) are listed in Table 1. Defining

$$q = \begin{cases} V_{max} & \text{if } W_c < W_j \\ \frac{2}{9}J & \text{if } W_c > W_j \end{cases} \tag{24}$$

and

$$K = \begin{cases} K_c\left(1 + \frac{p_o}{K_o}\right) & \text{if } W_c < W_j \\ \frac{7}{3}\Gamma & \text{if } W_c > W_j \end{cases} \tag{25}$$

expression (22) can be written in the more compact form

$$A = q\frac{C_i - \Gamma}{C_i + K} - R_d \tag{26}$$

Most of the variables defining photosynthesis depend on the leaf temperature T (measured in Kelvin). In order to quantify their temperature dependence we use the parametrisations given by Bernacchi et al. (2003) (see Appendix B.1).

We resume now the discussion of expression (20) from the end of Section 2.2. Having derived now a second relation between A and C_i we can use (20) and (26) to eliminate C_i from the function representing A. Equating expressions (20) and (26) leads to a quadratic equation for C_i with solution

$$C_i = \frac{1}{2g}\{g(C_a - K) - (q - R_d) \pm \sqrt{[g(C_a - K) - (q - R_d)]^2 + 4g(gKC_a + q\Gamma + KR_d)}\} \tag{27}$$

Since the solution with the minus sign in front of the root symbol leads to negative concentrations C_i we discard it. Employing the meaningful solution to eliminate C_i from Eq. (20) in favour of C_a and g we arrive at the following expression for the

Table 1
Parameters defining photosynthesis

Symbol	Unit	Quantity
A	μmol/m²/s	Assimilation rate per leaf area
J	μmol/m²/s	Rate of electron transport
J_{max}	μmol/m²/s	Maximum rate of electron transport
K_o	mmol/mol	Michaelis–Menten constant of oxygenation
K_c	μmol/mol	Michaelis–Menten constant of carboxylation
p_o	mmol/mol	Partial pressure of oxygen
Q	μmol/m²/s	Photosynthetic photon flux density
R_d	μmol/m²/s	Mitochondrial respiration rate in the light
V_{max}	μmol/m²/s	Maximum RuBP-saturated rate of carboxylation
W_c	μmol/m²/s	Rubisco limited rate of carboxylation
W_j	μmol/m²/s	RuBP-limited rate of carboxylation
α_l	–	Total leaf absorbance
β	–	Fraction of absorbed quanta reaching PSII
Γ	μmol/mol	CO_2-compensation point in the absence of dark respiration
Θ_{PSII}	–	Convexity term for electron transport rates
$\Phi_{PSII,max}$	–	Maximum dark-adapted quantum yield of PSII

assimilation rate:

$$A = \tfrac{1}{2}\{g(C_a + K) + (q - R_d) - \sqrt{[g(C_a - K) - (q - R_d)]^2 + 4g(gKC_a + q\Gamma + KR_d)}\} \tag{28}$$

2.4. Derivation of stomatal conductance from the optimisation principle

If the assimilation rate A is known, expression (28) can be solved for g which leads—in connection with definition (19)—to the desired relationship between v and C_a. In general, however, A is *not* known independently from (28). The information which is necessary to calculate $v(C_a)$ can, however, be supplied by an optimisation principle acting on the gas exchange described in Eqs. (21) and (28).

In habitats where water supply is not unlimited, it is imperative for plants to maximise assimilation while keeping the amount of transpired water low. It is generally assumed that stomata behave in an optimal way in order to maximise carbon gain while minimising transpiration (Cowan and Farquhar, 1977). Hari et al. (1986) and Mäkelä et al. (1996) suggested that plants optimise assimilation and transpiration in a way that takes into account diurnal or even seasonal changes of environmental conditions. An optimisation principle considering these aspects was successfully applied to stands of Scots Pine by Berninger et al. (1996) and *Pinus sylvestris* by Aalto and Juurola (2002). The rationale behind this optimisation scheme is that optimal behaviour has to take into account the availability of water (a plant cannot use more water in a certain time period than is available during this time period) and the influence of parameters like humidity, temperature and irradiance. Formally, such a behaviour can be expressed by the statements

$$\int_{\Delta t} A(t)\,\mathrm{d}t = \text{maximum} \tag{29}$$

and

$$\int_{\Delta t} E(t)\,\mathrm{d}t = W_0 \tag{30}$$

which have to be obeyed simultaneously (Mäkelä et al., 1996). Δt represents a reasonable time span (like one day or one season) and W_0 denotes the water supply (per leaf area) available during this time span. Furthermore, the parameters w_a, q, Γ, K and g appearing in expressions (21) and (28) for E and A depend either explicitly on time t, or implicitly via the time-dependent temperature $T(t)$.

Since a plant can regulate its stomatal conductance by adjusting stomatal density v or stomatal area a_{st} (or both) we consider the total conductance g which encompasses both effects (see Eq. (19)) as the variable whose temporal behaviour is to be calculated from the optimisation procedure. The time dependence of the quantities w_a, q, Γ and K are, however, assumed to be explicitly or implicitly prescribed.

In order to calculate the conductance $g(t)$ which maximises $\int_{\Delta t} A(t)\,\mathrm{d}t$ under the constraint $\int_{\Delta t} E(t)\,\mathrm{d}t = W_0$ we apply the method of Lagrangian multipliers (from the Calculus of Variation of Mathematical Physics, see e.g. Arfken, 1970, for slightly different formulations leading to the same results see Cowan, 1977; Cowan and Farquhar, 1977; Farquhar et al., 2002; Buckley et al., 2002; Mäkelä et al., 1996; Berninger et al., 1996). The optimisation procedure starts with forming the expression

$$\begin{aligned} L &= A - \lambda E \\ &= \frac{1}{2g}\{g(C_a + K) + (q - R_d) \\ &\quad - \sqrt{[g(C_a - K) - (q - R_d)]^2 + 4g(gKC_a + q\Gamma + KR_d)}\} \\ &\quad - \lambda a g(w_{sat} - w_a) \end{aligned} \tag{31}$$

where the second version emerges from substitution of A and E by expressions (28) and (21). (In mathematical terminology, the arbitrary constant λ is called the Lagrangian multiplier and $\int_{\Delta t} E(t)\,\mathrm{d}t = W_0$ is the constraint of the problem.) Then we calculate

$$\frac{\mathrm{d}}{\mathrm{d}t}\frac{\partial L}{\partial \dot{g}} = \frac{\partial L}{\partial g} \tag{32}$$

where $\dot{g} \equiv \mathrm{d}g/\mathrm{d}t$. The last equation constitutes an ordinary differential equation of second order for the conductance $g(t)$. Once the conductance $g(t)$ is known, the Lagrangian multiplier λ can—in principle—be calculated by evaluating the constraint $\int_{\Delta t} E(g(t))\,\mathrm{d}t = W_0$.

Inspection of expressions (28) and (21) shows that both A and E depend on g but neither of them depends on $\dot{g}$. Hence, Eq. (32) reduces to

$$0 = \frac{\partial L}{\partial g} \tag{33}$$

This implies two important simplifications: (i) the differential equation (32) of the generic case reduces to a mere algebraic equation for $g(t)$, and (ii) in order to solve Eq. (33) for $g(t)$ the time dependencies of the quantities w_a, q, Γ and K need not to be known explicitly.

Applying the optimisation scheme to Eq. (31) results in

$$\begin{aligned} g = \frac{1}{(C_a + K)^2}\Bigg\{ &\sqrt{\frac{q(K + \Gamma)[C_a(q - R_d) - (q\Gamma + KR_d)]}{[C_a + K - \lambda a(w_{sat} - w_a)]\lambda a(w_{sat} - w_a)}} \\ &\times [C_a + K - 2\lambda a(w_{sat} - w_a)] \\ &+ (q - R_d)C_a - (q\Gamma + KR_d) - q(K + \Gamma)\Bigg\} \end{aligned} \tag{34}$$

If the time-dependencies of insolation $Q(t)$, temperature $T(t)$ and atmospheric water vapour concentration $w_a(t)$ are explicitly known the constant λ (on which g depends) can be expressed in terms of the amount of water W_0 available during the time span Δt by inserting expression (34) into (21) and integrating the result according to (30). Since the photosynthetic parameters q, R_d, K and Γ vary via $T(t)$ also with time t, it is usually impossible to perform the integration in (30). From expression (30) it is, however, clear that λ is connected with water availability. The behaviour of $g(\lambda)$ (see Fig. 2) suggests that λ represents—at least in a loose sense—the "cost of water": small values of λ are related to high values of the optimum conductance g which indicates that high transpiration values are tolerable. This implies in turn that water is easily (without high costs) supplied. g is lower for higher values of λ, meaning that the necessity to avoid transpiration is more severe. In other words, water is more expensive.

It is possible to express λ in terms of quantities characterising the soil on which the tree grows and the hydraulic properties of its water transport system between roots and leaves. This is done in Appendix C.

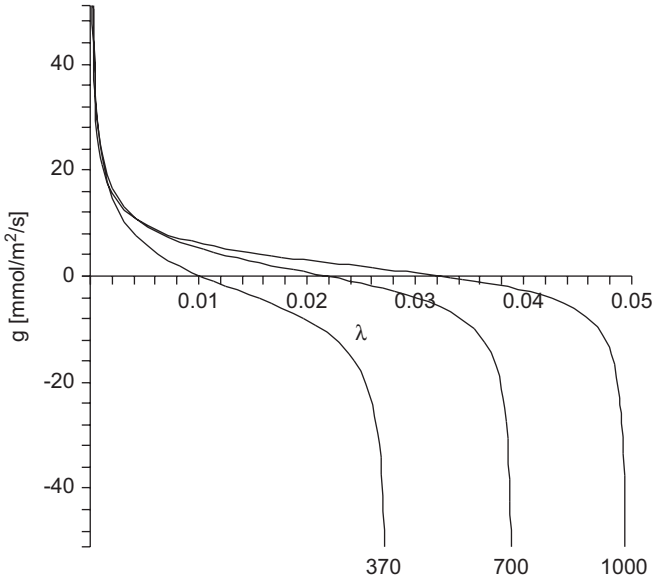

Fig. 2. Optimum conductance g as a function of the Lagrangian multiplier λ for $C_a = 370$, 700 and 1000 μmol/mol. Only values of λ between the pole at $\lambda = 0$ (common to the three curves) and their zeros (where the curves intersect the λ-axis) are meaningful since only they lead to positive values of the conductance g. The acceptable range of λ increases with the atmospheric CO_2 concentration C_a.

The optimum assimilation rate A related to g follows from substitution of expression (34) into Eq. (28)

$$A = \frac{1}{(C_a + K)}\left\{ C_a(q - R_d) - (q\Gamma + KR_d) - \sqrt{\frac{q(K+\Gamma)[C_a(q-R_d) - (q\Gamma + KR_d)]\lambda a(w_{sat} - w_a)}{(C_a + K - \lambda a(w_{sat} - w_a))}} \right\} \tag{35}$$

2.5. Relation between stomatal density and atmospheric CO_2

In order to obtain the desired $v(C_a)$-relationship, we insert (15) into (19) and solve for v

$$v = \frac{1}{a_{st}}\left(\frac{\left[d_{st}^{geom} + \sqrt{\frac{a_{st}}{\pi}} \right] g}{D_{CO_2} - \left[d_{bl} + d_{as}\frac{\tau_{as}^2}{n_{as}} \right] g} \right) \tag{36}$$

Then we substitute expression (12)

$$d_{bl} = 4 \times 10^{-3} \frac{m}{\sqrt{s}} \sqrt{\frac{l}{u_{wind}}}$$

and $g(C_a)$ from (34). The result is quite complex and the complexity increases if the temperature dependencies of the various parameters are included (see appendix).

In order to use (36) to exploit fossil values of v as a proxy for palaeoatmospheric C_a it is necessary to realise that two different time scales are involved in (36) which correspond to the two different options a plant has to regulate stomatal conductance $g(t)$: A plant can (i) open and close its stomata or it can (ii) create additional stomata, discard existing ones, and/or modify the dimensions of the stomatal pores (i.e. d_{st}^{geom}, w_{st}, h_{st}). Since the second option is related to morphological modifications, its realisation requires more time and expenditure than the first one. Hence, it is plausible to assume that (i) variations of stomatal aperture a_{st} are caused by the diurnal variations of temperature, insolation, atmospheric humidity and wind speed and by short-term variations of C_a while (ii) variations of v are due to long-term variations of the atmospheric CO_2-concentration. The time-scales of both variations differ by three orders of magnitude, i.e. they can be treated as being effectively independent of one another.

If we want ro reconstruct palaeoatmospheric CO_2 from fossil stomatal density we are interested only in the long-term variations of v. Hence, we have to separate both effects. This can be achieved as follows. The maximum stomatal area a_{st}^{max} corresponds to the maximum conductance g_{max} which may be temporarily realised if the partially interacting quantities solar insolation, temperature and humidity attain favourable values. Under such conditions relation (36) takes the form

$$v = \frac{1}{a_{st}^{max}}\left(\frac{\left[d_{st}^{geom} + \sqrt{\frac{a_{st}^{max}}{\pi}} \right] g_{max}}{D_{CO_2} - \left[d_{bl} + d_{as}\frac{\tau_{as}^2}{n_{as}} \right] g_{max}} \right) \tag{37}$$

with

$$d_{bl} = 4 \times 10^{-3} \frac{m}{\sqrt{s}} \sqrt{\frac{l}{u_{wind}}}$$

Principally, the (short-term) maximum conductance g_{max} and the time t_{max} when it occurs can be calculated from Eq. (34), provided the diurnal variations of insolation, temperature and humidity (resp. $Q(t)$, $T(t)$ and $w_{rel}(t)$, where $w_{rel} = w_a/w_{sat}$) are known (e.g. as illustrated by Fig. 5). Because the diurnal variation of g involves a much shorter time-scale than changes in stomatal density caused by changes in the atmospheric CO_2-concentration, C_a can be held constant when t_{max} is calculated. In principle, this can be done by first solving $dg/dt = 0$ for $t = t_{max}$ and then inserting t_{max} back into expression (34). The resulting relation $g_{max}(C_a)$ is not dependent on time. Substitution of $g_{max}(C_a)$ into (37) concludes the derivation of $v(C_a)$.

In reality, this course of action is not feasible because g is usually a very complicated function of t. We may, however, proceed as follows (in order to illustrate this procedure we refer to Figs. 3 and 4 which will be properly introduced and discussed in Section 3.2): Fig. 3 depicts the "mountain crests" of the functions $g(t, C_a)$ (upper row of Fig. 4) which represent the functions $g_{max}(C_a)$ used in (37). The curves indicate at what time of

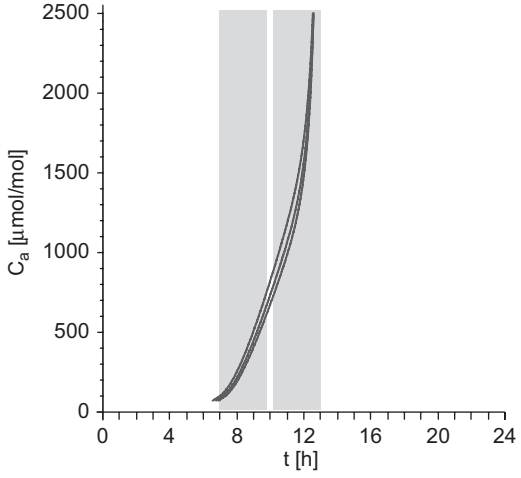

Fig. 3. Projections of the "mountain crests" of the functions $g(t, C_a)$ (upper row of Fig. 4) along the g-axis into the (t, C_a)-plane (corresponding—from right to left—to $\lambda = 0.0005$, 0.001 and 0.002). The curves indicate at what time of day—depending on C_a — the optimum stomatal conductance g attains its maximum value g_{max}. For $C_a \lessapprox 700$ μmol/mol this happens between $t \approx 7$ and 10 h, for $C_a \gtrapprox 700$ μmol/mol at a time between $t \approx 10$ and 13 h. The temporal intervals (grey areas) shown here are the same as in Fig. 5, depicting the diurnal variations of $Q(t)$, $T(t)$ and $w_{rel}(t)$. $t = 0$ and $t = 24$ denote midnight.

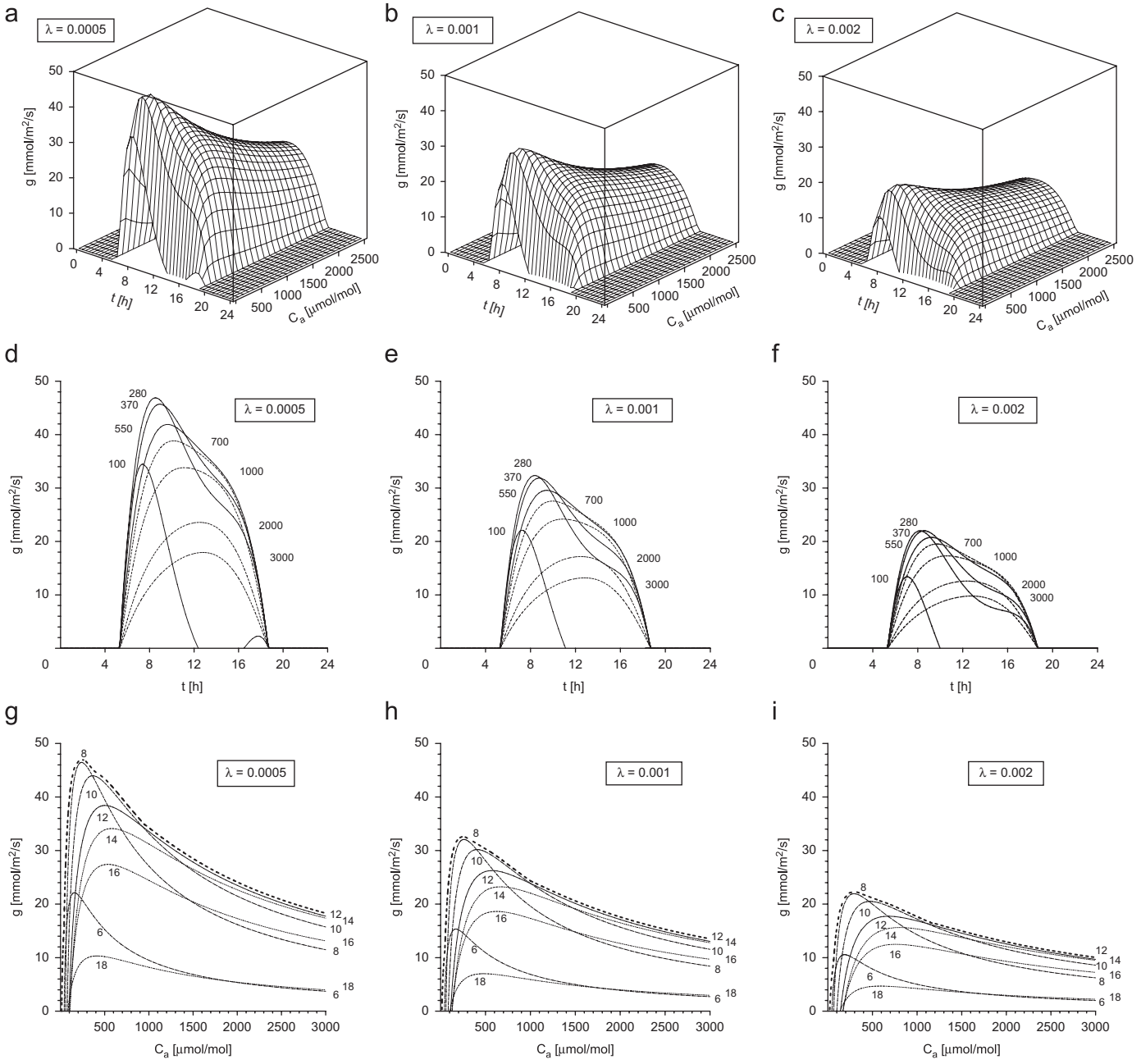

Fig. 4. *Upper row*: Conductance $g(t, C_a)$ as a function of t (diurnal variations) and atmospheric CO_2 concentration C_a for (a) $\lambda = 0.0005$, (b) $\lambda = 0.001$ and (c) $\lambda = 0.002$ (λ represents the cost of water). $g(t, C_a)$ is calculated according to (34) from diurnal variations of $Q(t)$, $T(t)$ and $w_a(t)$ as shown in Fig. 5. C_a is given in units of µmol/mol. $t = 0$ and 24 denote midnight. *Centre row*: Slices through the three-dimensional surfaces $g(t, C_a)$ of the upper row with C_a held constant. Numbers close to the maxima of the curves give C_a in units of µmol/mol (700, 1000, 2000 and 3000 µmol/mol correspond to the broken curves). Obviously, small values of λ (i.e. cheap water) are in favour of high values of optimum conductance g. *Lower row*: Slices through the three-dimensional surfaces $g(t, C_a)$ of the upper row with t held constant. Numbers close to the curves indicate the time of day. The assumption of darkness between 19 h in the evening and 5 h in the morning implies $g = 0$. Broken lines indicate the envelopes around the families of curves. The envelopes represent the functions $g_{max}(C_a)$ used in (37). Geometrically, they can be obtained by projecting the "crests" of the "mountains" of the upper row along the t-axis into the (g, C_a)-plane.

day—depending on C_a—the optimum stomatal conductance g attains its maximum value g_{max}. For $C_a \lessapprox 700$ µmol/mol this happens between $t \approx 7$ and 10 h, for $C_a \gtrapprox 700$ µmol/mol at a time between $t \approx 10$ and 13 h. Comparison of the grey areas in Fig. 3 with their counterparts in Fig. 5 allows to identify combinations of temperature and humidity ranges which correspond approximately to the maximum stomatal conductance. Insertion of these values of T and w_{rel} into (34) produces g_{max} which is then used in expression (37) in order to obtain $\nu(C_a)$.

Fig. 5 indicates also that maximum stomatal conductance is coupled with a high flux density Q of photosynthetic active photons. Then the first alternative of expressions (24) and (25) is valid, implying, that we need to know only two assimilation parameters explicitly in order to calculate g_{max}, namely $V_{\max,25\,^\circ C}$ and $R_{d,25\,^\circ C}$.

Summarising these results: In order to calculate stomatal density ν as a function of atmospheric CO_2 concentration C_a from Eq. (37) we need to know (or estimate) the following parameters:

(i) The assimilation parameters q, R_d, K and Γ.
(ii) The average of the diurnal temperature variation $T(t)$ during the vegetation period.

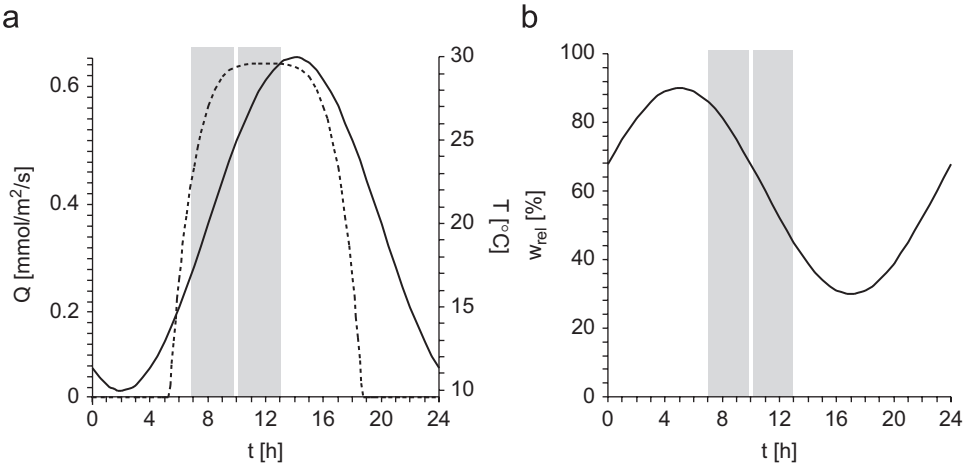

Fig. 5. Diurnal variations used as input functions for the stomatal conductance $g(t, C_a)$ shown in Fig. 4 ($t = 0$ and 24 h denote midnight): (a) photon flux density $Q(t)$ (dotted line) and temperature $T(t)$ (solid line) and (b) relative atmospheric humidity $w_{rel}(t)$. The input functions determine the time dependence of $g(t, C_a)$, either directly or via the temperature dependencies of the assimilation parameters q, R_d, K and Γ which occur in $g(t, C_a)$ (see (24), (25), (B.1) and (B.4)). The temporal intervals (grey areas) shown here are the same as in Fig. 3.

(iii) The average of the diurnal variation of the (relative) atmospheric humidity $w_{rel}(t)$ during the vegetation period.
(iv) The "cost of water" λ during the vegetation period.
(v) The average wind speed u_{wind} during the vegetation period.
(vi) The leaf anatomic parameters: maximum stomatal area a_{st}^{max}, depth of stomatal opening d_{st}^{geom}, thickness of assimilation tissue d_{as}, tortuosity of assimilation tissue τ_{as}, porosity of assimilation tissue n_{as} and average leaf length l (implying—together with u_{wind}—the thickness of the boundary layer d_{bl}).

In order to calculate g_{max} from (34) only the quantities (i)–(iv) are required. The first of these is species specific, the other three describe the environment.

The leaf anatomic parameters in (vi) can be obtained from fossil material. The value of a_{st}^{max}, however, has to be borrowed from extant counterparts by determining the maximum pore opening that is possible. Also the assimilation parameters in (i) have to be taken from an extant representative of the plant under consideration. The environmental parameters in (ii)–(v) are probably the most difficult to obtain because they are part of the climatic scenario one wants to unravel.

3. Exploration of model behaviour

3.1. Model parametrisation with G. biloba

The photosynthetic, environmental and anatomical parameters (and their sources) used to calculate $g(C_a)$-curves (from Eq. (34)) and $v(C_a)$-curves (from Eq. (37)) for *G. biloba* are provided in Table 2.

In the following it will be explained how the photosynthetic quantities and λ, the cost of water, have been obtained from measurements of physiological parameters of an adult *Ginkgo* in the field performed by Overdieck and Strassemeyer, 2005 (see Figs. 6 and 7 and Tables 3 and 4). These measurements were carried out at a temperature of $T = 27.3\,^{\circ}$C and at a relative atmospheric humidity of 50%.

3.1.1. Calculation of q, R_d, K and Γ

In order to calculate q, R_d, K and Γ we apply the method of least squares to Eq. (26)

$$A(C_i) = q\frac{C_i - \Gamma}{C_i + K} - R_d \tag{38}$$

q and K were defined in Eqs. (24) and (25). If the rate of carboxylation is limited by Rubisco activity and not by insolation—which we may assume in our case, see Fig. 5—they are given as $q = V_{max}$ and $K = K_c(1 + p_o/K_o)$. First, we form from Eq. (38) and the six data points $(C_{i,k}, A_k)$ of Table 3 the sum

$$\sigma_A^2 = \sum_k [A(C_{i,k}) - A_k]^2 \tag{39}$$

σ_A^2 constitutes a measure for the deviation of the curve $A(C_i)$ from the data points $(C_{i,k}, A_k)$, $(k = 1 \ldots 6)$. It depends on the four unknown quantities q, R_d, K and Γ. In order to obtain a "best fit" of the curve representing Eq. (38) to the data points, we have to locate the minimum of σ_A^2 ("nonlinear regression"). The minimum is characterised by the value of the quadruple (q, R_d, K, Γ) for which the four partial derivatives of σ_A^2 with respect to q, R_d, K and Γ vanish simultaneously. This system of four equations can be readily solved. Employing the temperature dependencies given by Bernacchi et al. (2003) in expressions (B.1) the solutions are normalised to the temperature $T = 25\,^{\circ}$C. For the results see Table 2. The dotted curve in Fig. 6 represents $A(C_i)$ emerging from reinsertion of the values representing the minimum of (39) into Eq. (38).

3.1.2. Calculation of λ

In order to proceed, we need a numeric value of the Lagrangian multiplier λ which represents the cost of water. As pointed out in Section 2.4, direct integration of Eq. (30) in order to express λ in terms of W_0, the amount of water available during the time Δt, is not possible. The method outlined in Appendix C, the derivation of λ from quantities characterising soil and plant water transport system would require detailed knowledge of the soil parameters and the ground water regime.

Fortunately, a third approach is feasible and successful because (i) Overdieck and Strassemeyer (2005) provide data relating $g_{sH_2O} = ag$ and C_a, and (ii) λ is the only still unknown quantity in expression (34) for $g(C_a)$. Proceeding similarly as above we use nonlinear regression in order to obtain a "best fit" of the curve $g_{s\,H_2O,}(C_a)$ to the six data points $(C_{a,k}, g_{s\,H_2O,k})$ $(k = 1 \ldots 6)$ given in

Table 2
Photosynthetic, environmental and anatomical parameters used to calculate $v(C_a)$ related to *Ginkgo biloba* and *Quercus petraea* from Eq. (37)

Symbol	*G. biloba*	*Q. petraea*	Unit	Quantity/Source/Remarks
Photosynthetic parameters				
q	4.28	22.6	$\mu mol/m^2/s$	See (26) and (B.1)[a]
R_d	0.11	0.39	$\mu mol/m^2/s$	See (26) and (B.1)[a]
K	205	464	$\mu mol/mol$	See (26) and (B.1)[a]
Γ	43	33	$\mu mol/mol$	See (26) and (B.1)[a]
$V_{max,25\,^\circ C}$	7.34	35.7	–	See (B.1)[a]
$R_{d,25\,^\circ C}$	0.16	0.54	–	See (B.1)[a]
$k_{25\,^\circ C}$	0.48	1	–	See(B.1)[a]
$\gamma_{25\,^\circ C}$	1.37	1	–	See (B.1)[a]
Environmental parameters				
u_{wind}	3	3	m/s	Wind speed[b]
w_{rel}	60	65	%	Relative atmospheric humidity[c]
T	19.07	20	°C	Temperature[c]
λ	1.57×10^{-3}	1.23×10^{-3}	–	"Cost of water"[a]
Anatomical parameters				
d_{st}^{geom}	31.9 ± 3.7	23	μm	Depth of stomatal opening (Fig. 1)[d]
w_{st}^{max}	1.2 ± 0.4	1.4	μm	Maximum width of stomatal opening[d]
h_{st}	13.1 ± 1.7	10.1	μm	Length of stomatal opening[d]
d_{as}	218 ± 32	100	μm	Thickness of assimilation tissue[d]
τ_{as}	1.571	1.571	–	Tortuosity of assimilation tissue[e]
n_{as}	0.35	0.33	–	Porosity of assimilation tissue[e]
l	84 ± 11	54	mm	Average leaf length[d]

Ginkgo biloba: The meaning of the superscripts in the last column is as follows:
[a]Calculated from Table 3.
[b]Rough estimate for Berlin.
[c]Average value for Berlin during growth period.
[d]Own measurements, Copeland (1902), Napp-Zinn (1966).
[e]Rough estimate.
The environmental parameters w_{rel}, T and λ are derived from data in Overdieck and Strassemeyer (2005). The photosynthetic quantities q, R_d, K and Γ refer to $T = 19.07\,^\circ C$. They are calculated from data provided in Overdieck and Strassemeyer (2005) via the expressions due to Bernacchi et al. (2003) as given in (B.1).
Quercus petraea: All data are taken from or derived from data in Kürschner (1996) and Kürschner et al. (1998).

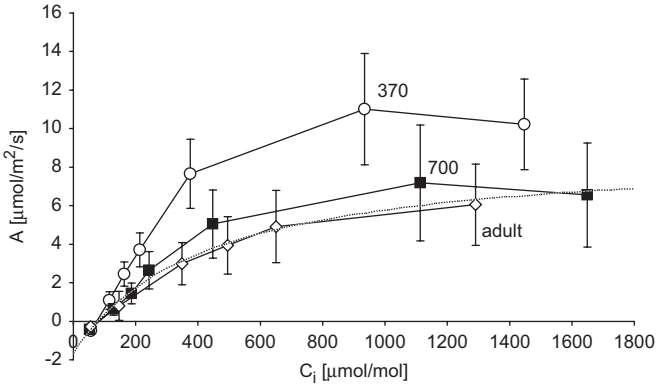

Fig. 6. Calculation of q, R_d, K and Γ from data points included in Figs. 1 and 2 of Overdieck and Strassemeyer (2005). The data are related to three groups of *Ginkgo biloba* plants. Open circles: Saplings grown for 2 years at $C_a \approx 370\,\mu mol/mol$. *Black squares*: Saplings grown for 2 years at $C_a \approx 700\,\mu mol/mol$. *Open squares*: Values of an adult *Ginkgo biloba* growing in the field (Berlin) at $C_a \approx 370\,\mu mol/mol$. The dotted curve represents the function $A(C_i)$ (see (38)). q, R_d, K and Γ were obtained by the least squares method according to (39) from the (C_i, A) data pairs in Table 3.

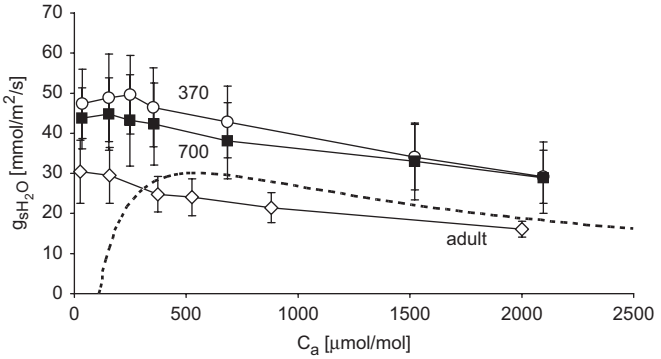

Fig. 7. Calculation of λ from data points included in Figs. 1 and 2 of Overdieck and Strassemeyer, 2005. The data are related to three groups of *Ginkgo biloba* plants. *Open circles*: Saplings grown for 2 years at $C_a \approx 370\,\mu mol/mol$. *Filled diamonds*: Saplings grown for 2 years at $C_a \approx 700\,\mu mol/mol$. *Open squares*: Values of an adult *Ginkgo biloba* growing in the field (Berlin) at $C_a \approx 370\,\mu mol/mol$. The dotted curve represents the function $g_{s\,H_2O}(C_a)$. λ was obtained by the least squares method (according to (40)) from the $(C_a, g_{s\,H_2O,})$ data pairs of Table 4.

Table 4. Using the relation $g_{s\,H_2O,} = ag$ (with $a = D_{H_2O}/D_{CO_2}$) we start with the expression

$$\sigma_g^2 = \sum_k [ag(C_{a,k}) - g_k]^2 \tag{40}$$

which depends on λ, the only parameter in $g(C_a)$ which is not yet fixed. Calculating a "best fit" of the curve representing Eq. (34) to

Table 3
Data pairs (C_i, A) from Overdieck and Strassemeyer (2005) used to calculate the quantities (q, R_d, K, Γ) via the least squares method

C_i	55.5	145	340	492	647	1287	$\mu mol/mol$
A	−0.26	0.81	3.13	3.93	4.9	6.11	$\mu mol/m^2/s$

The data were obtained at a temperature $T = 27.3\,^\circ C$ and a relative atmospheric humidity of 50%.

Table 4
Data points (C_a, g_{sH_2O}) from Overdieck and Strassemeyer (2005) used to calculate the "cost of water" λ via the least squares method

C_a	25	163	375	525	875	2000	μmol/mol
g_{sH_2O}	31	29	25	24	22	17	mmol/m²/s

The data were obtained at a temperature $T = 27.3\,^{\circ}C$ and a relative atmospheric humidity of 50%.

the data points similarly as in Section 3.1.1, the minimum of σ_g^2 is found at $\lambda = 1.57 \times 10^{-3}$. The dotted curve in Fig. 7 represents $g_{sH_2O}(C_a) = ag(C_a)$ obtained from this value for λ (B.1).

3.2. Basic model features

In the following, the basic features of the model are demonstrated. Although these features are in principle species independent we need numerical parameter values in order to illustrate

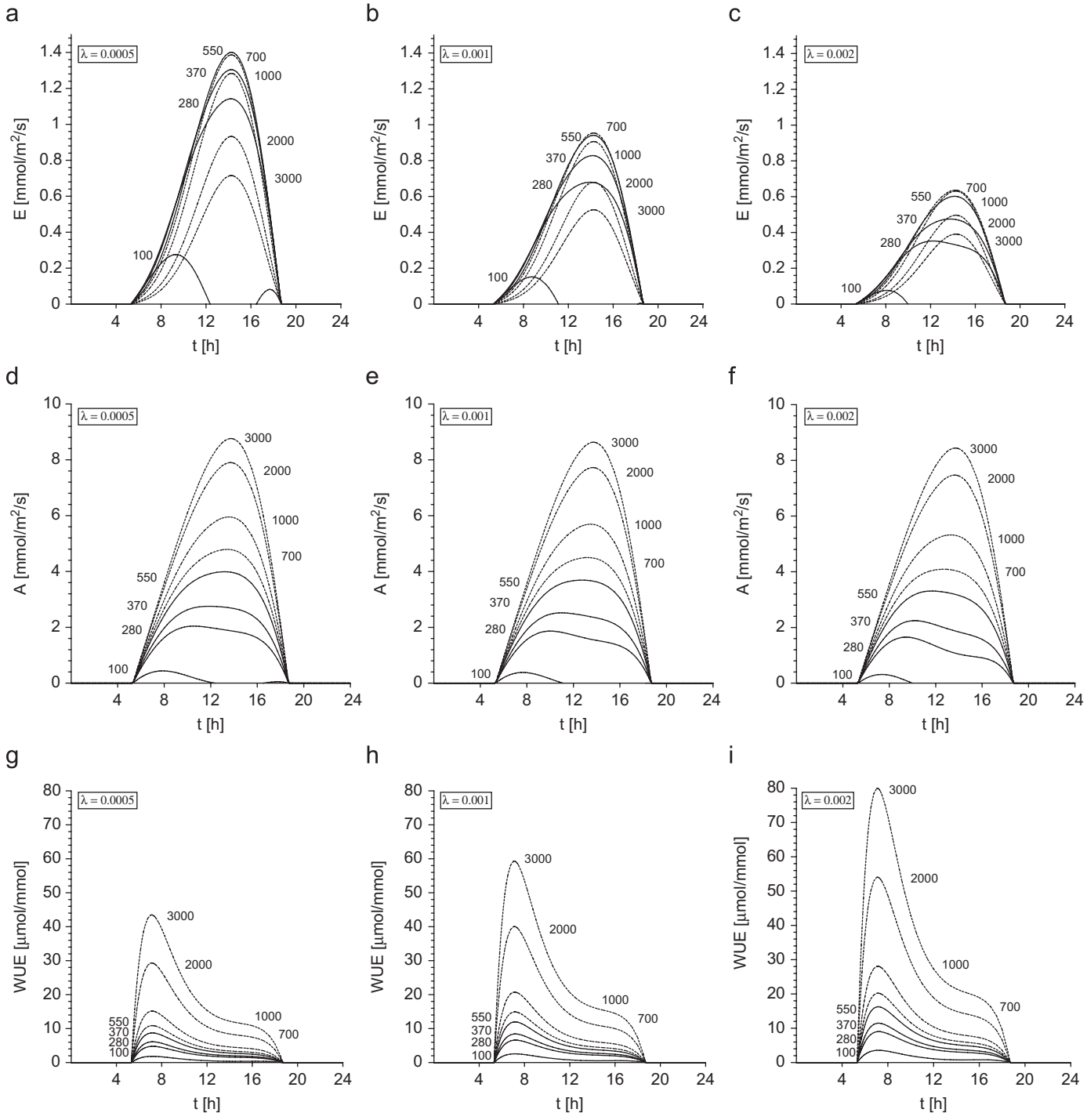

Fig. 8. Transpiration rate $E(t)$ (a,b,c), assimilation rate $A(t)$ (d,e,f) and water use efficiency $WUE(t) = A(t)/E(t)$ (g,h,i) as a function of t (diurnal variations) for various values of the cost of water λ. $E(t)$, $A(t)$ and $WUE(t)$ are calculated according to (21) and (35) from the diurnal variations of $Q(t)$, $T(t)$ and $w_a(t)$ shown in Fig. 5. The atmospheric CO_2 concentration C_a is held constant along each curve. Numbers close to the maxima of the curves give C_a in units of μmol/mol (700, 1000, 2000 and 3000 μmol/mol correspond to the broken curves). C_a is given in units of μmol/mol. $t = 0$ and 24 h denote midnight.

them. We use the parameters listed in Table 2 for *G. biloba* which were obtained in Sections 3.1.1 and 3.1.2. Additionally, we use the input functions depicted in Fig. 5 reflecting realistic diurnal variations of insolation $Q(t)$, temperature $T(t)$ and atmospheric water vapour concentration $w_{rel}(t)$ for a warm weather period during July 1991 in Berlin (Senatsverwaltung für Stadtentwicklung Berlin, 1993).

Figs. 4 and 8 show how the diurnal variations of conductance $g(t)$, assimilation rate $A(t)$, transpiration rate $E(t)$ and water use efficiency $WUE(t) = A(t)/E(t)$ depend on the cost of water λ and on the atmospheric CO_2 concentration C_a. Figs. 4(d)–(i) and 8 consist of families of curves which are generated by assigning the following C_a-values: $C_a = 100$ and $280\,\mu mol/mol$ (preindustrial CO_2-level), $C_a = 370\,\mu mol/mol$ (today's value), $C_a = 550\,\mu mol/mol$ (around year 2050), $C_a = 700\,\mu mol/mol$ (around year 2100), $C_a = 1000\,\mu mol/mol$ (Eocene, see Pagani et al., 2005), $C_a = 2000\,\mu mol/mol$ (Eocene, see Pagani et al., 2005), $C_a = 3000\,\mu mol/mol$ (Lower Devonian, see Berner and Kothvala, 2001) (for the predictions for the years 2050 and 2100 see Prentice et al., 2001). The following features of these curves are noteworthy:

- $g(t)$ and $E(t)$ decrease with increasing λ, $A(t)$, however, is nearly unaffected. Clearly, this asymmetry entails that $WUE(t) = A(t)/E(t)$ increases along with λ, as is to be expected from the interpretation of λ as the cost of water. Mathematically, the different sensitivities of $A(t)$ and $E(t)$ with respect to λ can be understood from expressions (D.1) and (D.2), the series expansions of both quantities with respect to λ: for small values of λ the expansion of $A(t)$ is dominated by a constant term, while the expansion of $E(t)$ is dominated by a term proportional to $1/\sqrt{\lambda}$. Hence, variations in λ affect $A(t)$ only weakly, $E(t)$, however, strongly.
- The value of λ affects the maximum values, but does not alter significantly the shape of the curves $g(t)$, $g(C_a)$, $E(t)$, $A(t)$ and $WUE(t)$.
- The curves g, E and A in Fig. 9 indicate more clearly a feature already included in Figs. 4 and 8: Although both E and A are calculated via expressions (34) and (35) from the optimum stomatal conductance g, only E inherits the maximum of g with respect to C_a. Depending on the values of λ and t, it is located within the range $C_a \approx 100 \ldots 800\,\mu mol/mol$. (Since E is—with respect to the variable C_a—simply a multiple of g (see Eq. (21)), the maxima of both functions are necessarily located at the same value of C_a.) $A(C_a)$, however, increases monotonically with C_a.
- The midday depressions of $g(t)$, $E(t)$, $A(t)$ and $WUE(t)$ become more distinct with decreasing C_a. With $A(t)$ and $WUE(t)$ they are much less pronounced than with $g(t)$ and $E(t)$.
- In the FACE-experiments (Long et al., 2004; Ainsworth and Long, 2005) it has been found that the stomatal conductance g of C_3-plants decreases by about 20% while their assimilation rate A increases by 30%...50% if the atmospheric CO_2 is raised from the recent value of $C_a = 370$ to $C_a = 550\,\mu mol/mol$ (to be expected to occur around the year 2050). The predictions from the model are in accordance with both observations: Calculating the model responses for this C_a-increase from the input values of Table 2 we find for the relative changes of stomatal conductance and assimilation $\Delta g/g = -11\%$ and $\Delta A/A = 21\%$, respectively.

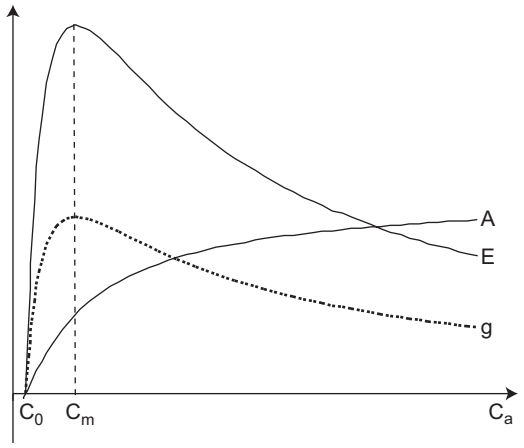

Fig. 9. Principal behaviour of optimum conductance g, assimilation rate A and transpiration rate E as a function of atmospheric C_a according to expressions (34), (21) and (35). A increases steadily with increasing C_a, although g and E show distinctive maxima at $C_a = C_m$ and decrease beyond their maxima. All three functions become zero at $C_a = C_0$.

Due to the structure of expression (36), the functions $g(C_a)$ and $v(C_a)$ share many properties in the range $C_a > 0$ (for details, consult Appendix E).

3.3. Sensitivity studies: identification of critical parameters

If the model is applied to reconstruct fossil C_a, errors can arise especially from the following sources: (i) from the high natural variance of stomatal data, (ii) from limited amount of knowledge about climatic parameters which existed when the fossil plants grew, (iii) from missing data concerning other leaf anatomical traits and (iv) from the necessity to use extant physiological data. Thus, it is necessary to explore to what extent uncertainties in the photosynthetic, environmental and anatomical parameters influence the $v(C_a)$-curves obtained from Eq. (37): if reliable results are desired, the most sensitive parameters should be known with great accuracy, for the less sensitive parameters rough estimates of their values may be sufficient (sensitivity means that small deviations in a parameter value cause large deviations in the stomatal density v). This can be achieved by performing sensitivity studies, in which the model parameters are varied systematically.

A set of curves was calculated for *G. biloba* by assigning various values to one of the input parameters (denoted by ξ) while keeping the other parameters constant. The constant values of the parameters are listed in Table 2. Comparison of the $v(C_a;\xi)$-curves allows to identify the most sensitive parameters.

3.3.1. Sensitivity of $v(C_a)$ against fluctuations of the photosynthetic parameters

Fig. 10 shows that the stomatal density v is most sensitive against variations of the parameter q (defined in (24)). An increase in q shifts the C_a that is signalled by a certain v to significantly higher values. Variations in K (defined in (25)) produce a much smaller change of v, and the effects of varying R_d and Γ are—compared with q—almost negligible. q has therefore to be considered as a very critical parameter.

3.3.2. Sensitivity of $v(C_a)$ against fluctuations of the environmental parameters

Of the environmental parameters, the wind speed u_{wind} has the least impact on v (see Fig. 11). The curves $v(C_a;u_{wind})$ are virtually indistinguishable for a very wide range of wind speeds. Only if u_{wind} approaches zero $v(C_a;u_{wind})$ increases somewhat. Variations in (relative) atmospheric humidity w_{rel}, cost of water λ or temperature T cause, however, effects which should not be neglected: the maxima of both $v(C_a;w_{rel})$ and $v(C_a;\lambda)$ increase and become sharper if humidity increases resp. if water becomes

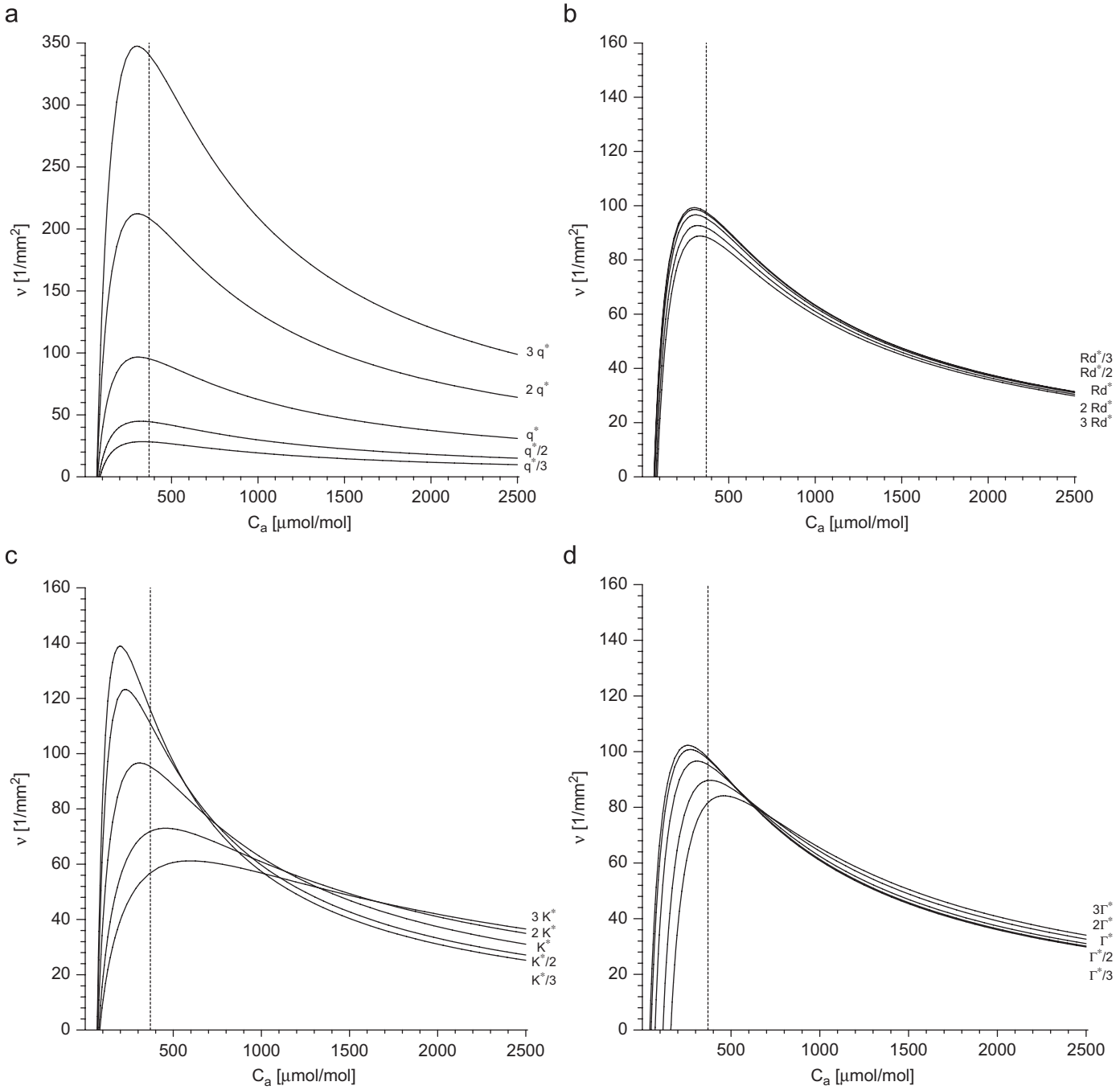

Fig. 10. Dependence of $\nu(C_a;\xi)$-curves on the photosynthetic parameters $\xi = q, R_d, K$ and Γ. Parameters are as in Table 2 and related to the adult *Ginkgo biloba* tree investigated in Overdieck and Strassemeyer (2005) in Berlin. Each family of $\nu(C_a;\xi)$-curves is generated by substituting $\xi = \xi^*/3, \xi^*/2, \xi^*, 2\,\xi^*, 3\,\xi^*$ into Eq. (37) where ξ^* is the parameter value given in Table 2. The present atmospheric CO_2 concentration $C_a \approx 370\,\mu\text{mol/mol}$ is indicated by vertical broken lines: (a) $\nu(C_a;q)$, (b) $\nu(C_a;R_d)$, (c) $\nu(C_a;K)$ and (d) $\nu(C_a;\Gamma)$.

cheaper. If the temperature T increases, the maxima of $\nu(C_a;T)$ also increase, they become, however, less pronounced and shift to higher C_a-values (Fig. 11).

Fig. 13 shows the behaviour of the $\nu(C_a)$-curves for a much wider range of combinations of temperature T and relative humidity w_{rel} than those presented in Figs. 11(a) and (c). The range of C_a is confined to the interval $C_a = 0\ldots600\,\mu\text{mol/mol}$, including the quaternary CO_2 minimum ($C_a \approx 180\,\mu\text{mol/mol}$, Beerling et al., 1995), the present atmospheric CO_2 ($C_a \approx 370\,\mu\text{mol/mol}$) and the atmospheric CO_2 to be expected to occur around the year 2050 ($C_a \approx 550\,\mu\text{mol/mol}$). Fig. 13 demonstrates that the position of the maximum of $\nu(C_a)$ is dependent on environmental parameters and that ν can attain much higher values than those which are usually observed under present conditions.

3.3.3. Sensitivity of $\nu(C_a)$ against fluctuations of the anatomical parameters

With decreasing maximum pore area a_{st}^{max}, the maximum of the $\nu(C_a)$-curve increases strongly to higher ν-values (see Fig. 12). Hence, the maximum pore area a_{st}^{max} has fundamental influence on the $\nu(C_a)$-relation. Under a pore area $a_{st}^{max} = 10\,\mu\text{m}^2$, for example, stomatal density $\nu = 105/\text{mm}^2$ implies an atmospheric CO_2

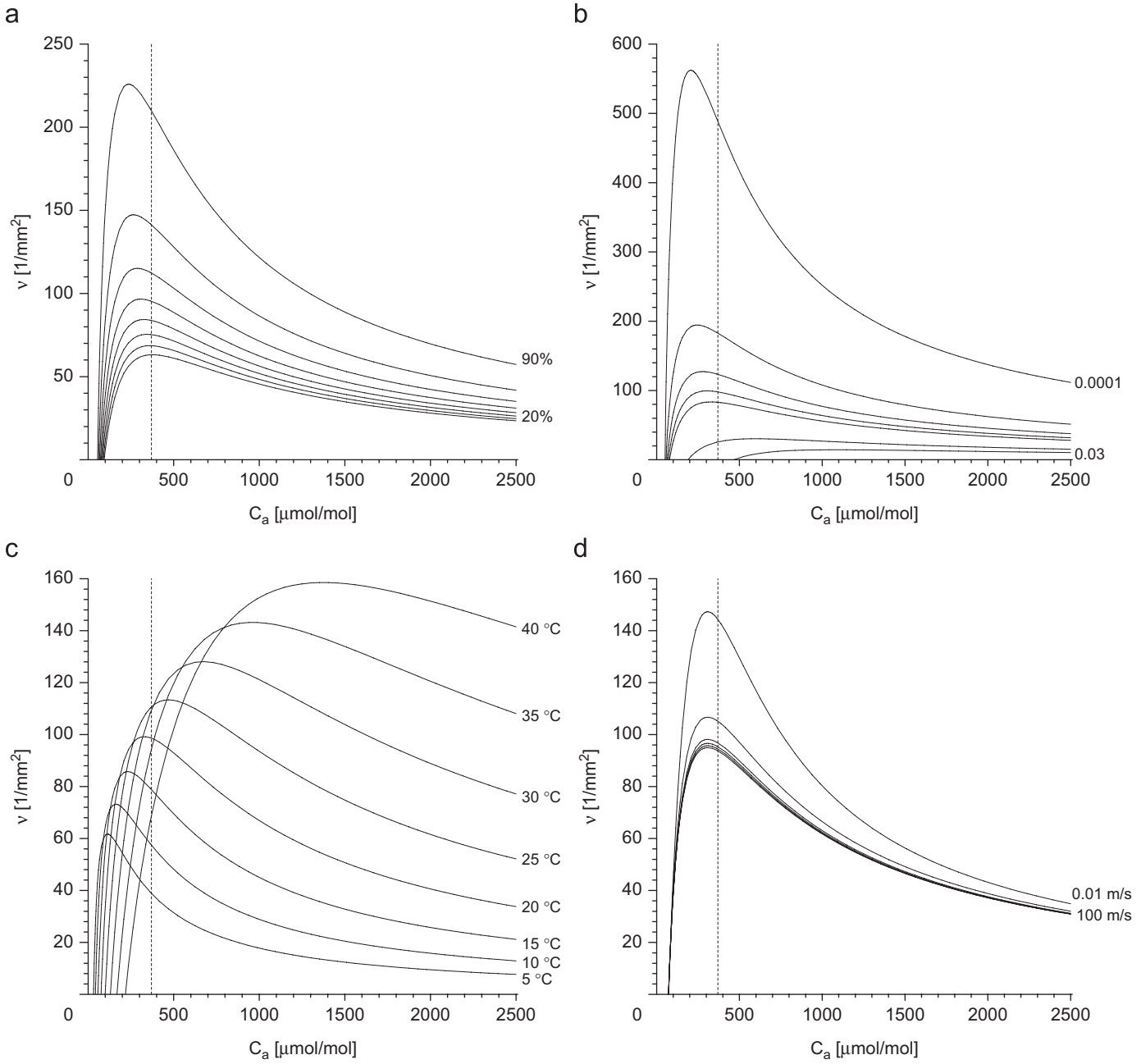

Fig. 11. Dependence of $v(C_a;\xi)$-curves on the environmental parameters atmospheric humidity, cost of water, temperature, and wind speed. Parameters used (except those which are varied) are as in Table 2 and related to the adult *Ginkgo biloba* tree investigated in Overdieck and Strassemeyer (2005) in Berlin. Values of varied quantities are indicated by the labels to the right of the curves. The present atmospheric CO_2 concentration $C_a \approx 370\,\mu\text{mol/mol}$ is indicated by a vertical broken line. (a) The (relative) atmospheric humidity varies from 20% to 90% in steps of 10% ($v(C_a;w_{rel})$, w_{rel}: atmospheric humidity). (b) The cost of water varies. $\lambda = 0.0001, 0.0005, 0.001, 0.0015, 0.002, 0.01$ and 0.03 ($v(C_a;\lambda)$, λ: cost of water). (c) The temperature varies from 5 to 40 °C in steps of 5 °C ($v(C_a;T)$, T: temperature) and (d) The wind speed is varied. Values of u_{wind} are 0.01, 0.1, 1, 3, 10, 100 m/s (from upper- to lower-most curve) ($v(C_a;u_{wind})$, u_{wind}: wind speed).

concentration of $C_a = 370\,\mu\text{mol/mol}$. With pore areas $a_{st}^{max} = 8\,\mu\text{m}^2$, $a_{st}^{max} = 6\,\mu\text{m}^2$ or $a_{st}^{max} = 4\,\mu\text{m}^2$ the same stomatal density implies, however, $C_a = 720$, 1160 and $C_a = 1970\,\mu\text{mol/mol}$, respectively. A comparable effect results if the stomatal depth d_{st} is increased. In attempts to reconstruct palaeoatmospheric CO_2 from fossil stomatal density it is thus necessary to include information about maximum stomatal pore size and stomatal depth. In the case of *G. biloba*, there are indications that stomatal dimensions tend to increase from late Miocene to Pliocene (Denk and Velitzelos, 2002).

Inspection of Fig. 12 reveals that the other anatomical parameters describing the assimilating tissue (i.e. d_{as}, t_{as}, n_{as}) do not strongly influence the $v(C_a)$-curve. Still less important is the leaf length l (see Fig. 12).

3.4. Model parametrisation with Quercus petraea

In order to check the model behaviour for a different species, it is also applied to *Q. petraea*. This species was also repeatedly used for reconstructing C_a values of the past (Kürschner, 1996; Kürschner et al., 1998). The input parameters related to this species (see Table 2) lead to $v(C_a)$-curves which exhibit the same patterns as those obtained for *G. biloba*. (i) $v(C_a)$-curves show for

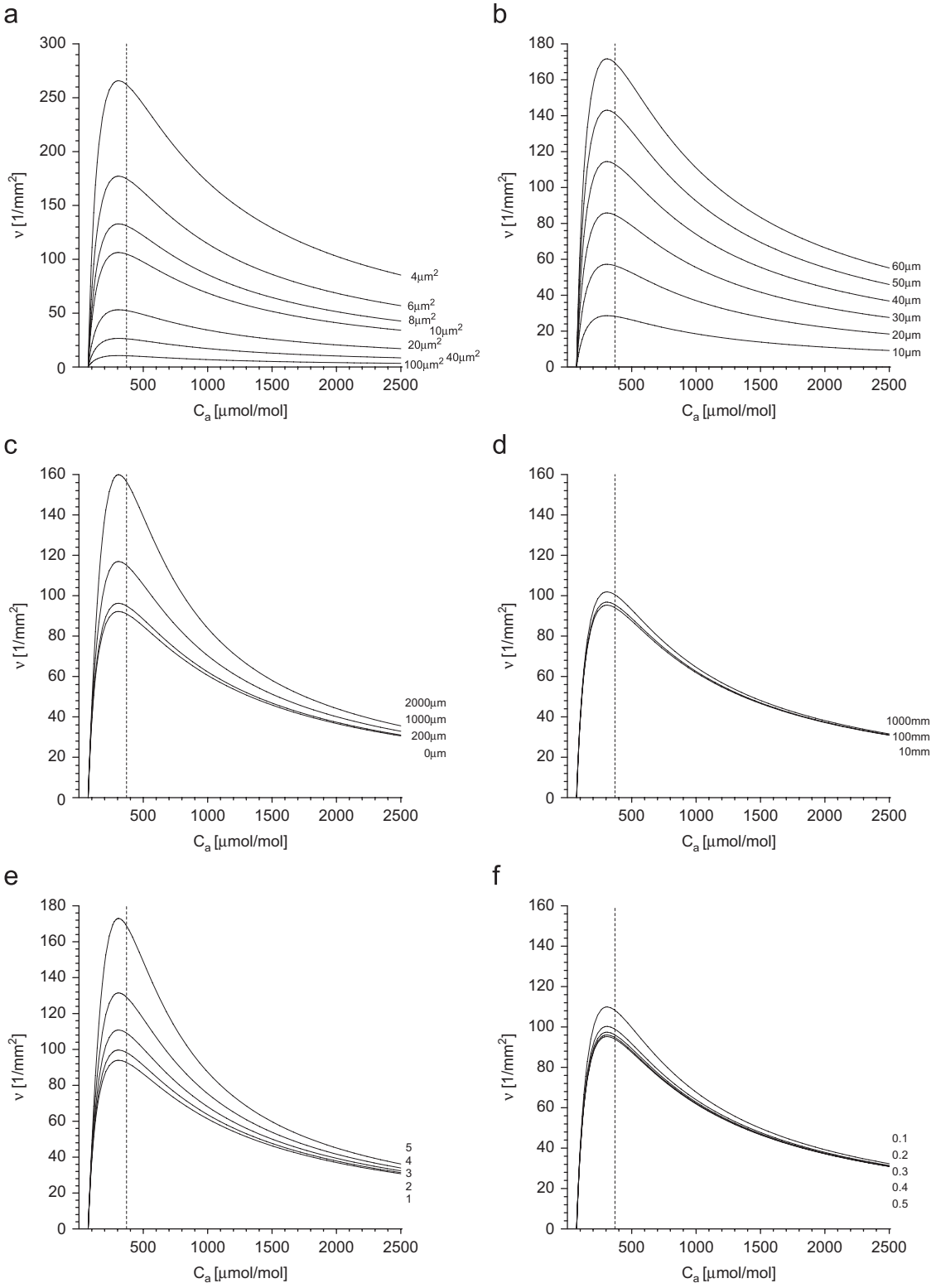

Fig. 12. Dependence of $\nu(C_a)$-curves on the anatomical parameters. Parameters used (except those which are varied) are as in Table 2 and related to the adult *Ginkgo biloba* tree investigated in Overdieck and Strassemeyer (2005) in Berlin. Values of varied quantities are indicated by the labels to the right of the curves. The present atmospheric CO_2 concentration $C_a \approx 370\,\mu\text{mol/mol}$ is indicated by a vertical broken line: (a) $\nu(C_a; a_{st})$, a_{st}: stomatal area; (b) $\nu(C_a; d_{st})$, d_{st}: depth of stomatal pore; (c) $\nu(C_a; d_{as})$, d_{as}: thickness of assimilating tissue; (d) $\nu(C_a; l)$, l: length of a leaf; (e) $\nu(C_a; t_{as})$, t_{as}: tortuosity of assimilating tissue and (f) $\nu(C_a; n_{as})$, n_{as}: porosity of assimilating tissue.

both species the same responses with respect to shifts of the positions of the maxima when photosynthetic, environmental or leaf morphological parameters are varied. (ii) Sensitivity studies lead to the same hierarchy of critical parameters. Hence, we restrict the representation of the results obtained with *Q. petraea* to Fig. 14 which shows $\nu(C_a)$-curves resulting from variation of both temperature T and relative humidity w_{rel} (as are described in Section 3.3.2).

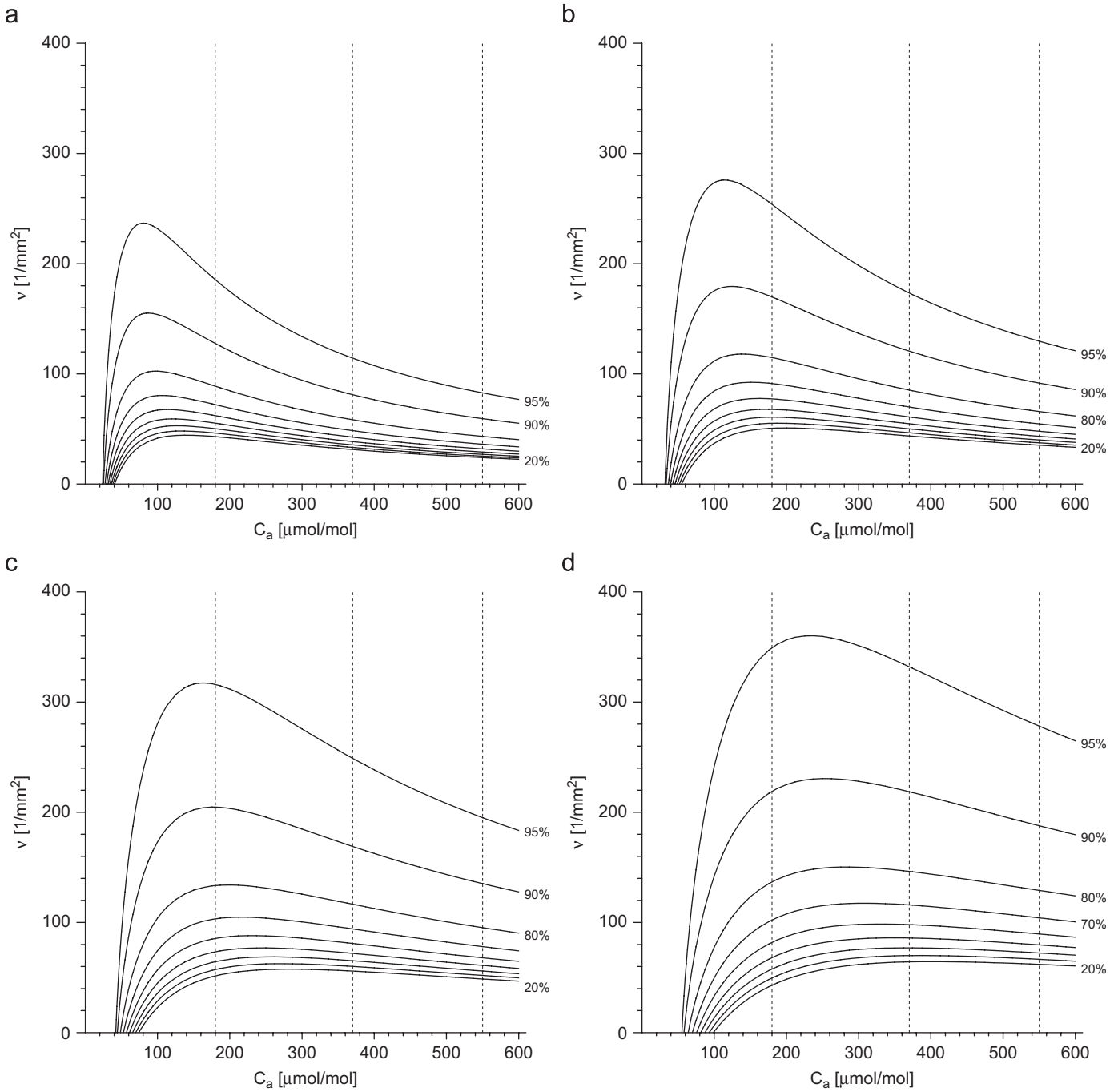

Fig. 13. Dependence of $v(C_a; w_{rel})$-curves on temperature. Parameters refer to *Ginkgo biloba* (see Table 2). The (relative) atmospheric humidity varies in steps of 10% between 20% to 90%. The atmospheric CO_2 concentrations of the quaternary minimum ($C_a \approx 180\,\mu$mol/mol), of the present ($C_a \approx 370\,\mu$mol/mol) and a prediction for the year 2050 ($C_a \approx 550\,\mu$mol/mol) are indicated by vertical broken lines: (a) $v(C_a; w_{rel})$, $T = 5\,^{\circ}$C; (b) $v(C_a; w_{rel})$, $T = 10\,^{\circ}$C; (c) $v(C_a; w_{rel})$, $T = 15\,^{\circ}$C and (d) $v(C_a; w_{rel})$, $T = 20\,^{\circ}$C.

4. Final considerations

The model presented in this contribution is based on an optimisation principle about the optimum use of the resource materials CO_2 and water and reflects the daily course of stomatal conductance which is usually due to stomatal aperture change. This approach was expanded in this paper by introducing structural data (e.g. stomatal density and pore area) which influence stomatal conductance on a fundamentally different time scale. This is possible because the optimisation principle holds also for structural parameters: if structural changes provide for an improvement under changing C_a and certain environmental conditions and if these changes cannot be realised by a phenotypic response, then these changes will occur during an evolutionary process which favours those genotypes which express the suitable adaptations. In fact, the differences in phenotypic $v(C_a)$ response can be large within a taxon for different genotypes, as demonstrated for different accessions of *Arabidopsis thaliana* (Woodward et al., 2002) and *Nothofagus cunninghamii* (Hovenden and Schimanski, 2000).

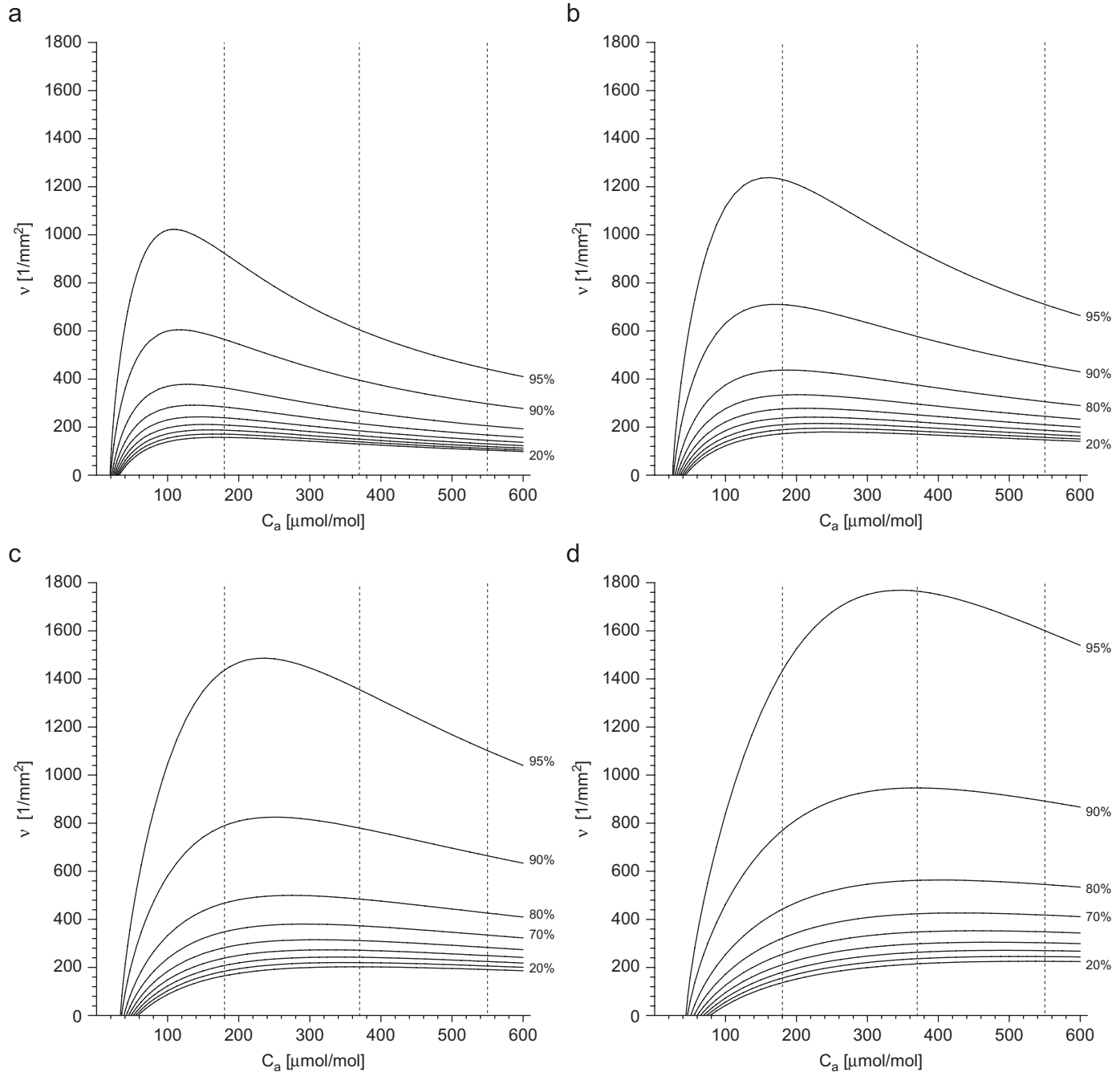

Fig. 14. Dependence of $\nu(C_a; w_{rel})$-curves on temperature. Parameters refer to *Quercus petraea* (see Table 2). The (relative) atmospheric humidity varies in steps of 10% between 20% to 90%. The atmospheric CO_2 concentrations of the quaternary minimum ($C_a \approx 180\,\mu$mol/mol), of the present ($C_a \approx 370\,\mu$mol/mol) and a prediction for the year 2050 ($C_a \approx 550\,\mu$mol/mol) are indicated by vertical broken lines: (a) $\nu(C_a; w_{rel})$, $T = 5\,^{\circ}$C; (b) $\nu(C_a; w_{rel})$, $T = 10\,^{\circ}$C; (c) $\nu(C_a; w_{rel})$, $T = 15\,^{\circ}$C and (d) $\nu(C_a; w_{rel})$, $T = 20\,^{\circ}$C.

The sensitivity analysis revealed both critical and non-critical parameters: critical parameters with respect to the $\nu(C_a)$ response are the photosynthetic parameters q (and, of secondary importance, K), (relative) atmospheric humidity w_{rel}, the cost of water λ and the temperature T, pore area a_{st} and depth d_{st} of the stomatal pore. The dominance of the environmental parameters which indicate the availability of water reflects the tight coupling between assimilation and transpiration. There are numerous indications for a tight coupling between water availability, water conduction and gas exchange (Katul et al., 2003). The various aspects of humidity (air humidity, soil water potential and soil type, precipitation) have therefore significant influence upon evolutionary $\nu(C_a)$-responses.

Plant response to increasing C_a is also affected by nutrient supply and metabolism, especially nitrogen (Reich et al., 2006). The general observation made in experiments under elevated C_a is that—on the leaf level—net assimilation increases while stomatal conductance and nitrogen content of leaves decrease (Ainsworth and Long, 2005; Ainsworth and Rogers, 2007). Furthermore, a decrease in V_{max} and J_{max} can be often observed (Ainsworth and Long, 2005; Ainsworth and Rogers, 2007). Apparently, trees show a low degree of photosynthesis acclimation, with a V_{max} decrease

of about 6%...10% and a J_{max} decrease close to zero (Medlyn et al., 1999; Ainsworth and Rogers, 2007). There is evidence that this down-regulation of the photosynthesis apparatus is enhanced under low N availability (Stitt and Krapp, 1999). This means that the C_a response will be affected also by environmental conditions involved in nutrient supply. In fact, plants grown under low N tend to show a greater decrease of V_{max} and J_{max} (Ainsworth and Long, 2005). It is therefore to be expected that the long-term effect of C_a on plants is also influenced by N availability. For reconstruction of C_a with stomatal data, it would be therefore desirable to incorporate this effect into the model although it is difficult to estimate N availability in the case of fossil environments. Another possibility would be to perform a sensitivity analysis which includes down-regulation of photosynthesis parameters under low N on the basis of the data set that is available so far.

The $v(C_a)$-response obtained from expression (37) is strongly influenced by other environmental parameters such as temperature or atmospheric humidity. Hence, inferring palaeoatmospheric C_a from fossil stomatal density v without taking possible modulations from the environment into account may be misleading. Reconstruction of palaeoatmospheric CO_2 by using the $v(C_a)$-response should therefore be accompanied by palaeoclimatic studies revealing parameters such as humidity and mean temperature during the growth period of the sites which are under consideration. The obtained values of palaeoclimatic parameters are then entered directly into the model. Palaeoclimatic studies may only provide parameter values which are highly uncertain. If such a parameter is critical with respect to the sensitivity of the model it is possible to insert the endpoints of its most probable range of values into the model. The model produces then a corresponding "envelope" of $v(C_a)$-curves.

Acknowledgements

Parts of the work were carried out within a visit to the National Museum for Natural History, Stockholm, Sweden, funded by the HIGHLAT programme (W.K. and A.R.-N.), which is gratefully acknowledged. We thank an anonymous reviewer for helpful comments and James Nebelsick, Tübingen, for critically reading the English manuscript.

Appendix A. Approximations

A.1. The porous medium approximation

The porous medium approximation is widely used to describe processes which take place in porous media (Aris, 1975) and in plant leaf tissue (see Parkhurst and Mott, 1990 and the review Parkhurst, 1994 and literature cited therein). Its central idea is the replacement of the discontinuous arrangement of cells and voids inside the real plant by a fictitious tissue whose continuous material properties are partly attributable to the cells and partly to the voids of the real plant. This is achieved by an averaging process which reduces the complex geometrical details of the cell and void architecture to just two quantities, the porosity n and the tortuosity τ, defined by

$$n := \frac{V_p}{V} \quad \text{and} \quad \tau := \frac{l_e}{l} \tag{A.1}$$

V_p and V are pore volume resp. total volume of a volume element. l_e denotes the length of the actual path which a molecule has to follow in order to move from one given point to another and l denotes the (geometrically) shortest distance between these same points. The effective conductance S is defined in terms of n, τ and the free air coefficient of diffusion D as

$$S := D\,\frac{n}{\tau^2} \tag{A.2}$$

Notice, that $D = D_{CO_2}$ or D_{H_2O}, depending on whether diffusion of CO_2 or H_2O molecules is considered.

A.2. Constancy of effective conductance

Plant leaves consist of several tissue layers (see stomatal and assimilation layers in Fig. 1). Due to the anatomical structure of leaves, porosity n and tortuosity τ change more or less abruptly between adjacent layers, but vary only slightly within the individual layers. The effective conductance S (defined in (A.2)) should behave similarly, i.e. $S = \text{const.}$ *within* a given layer.

A.3. Stationary conditions

We focus on stationary situations, i.e. we assume that the term $\partial c/\partial t$ on the right-hand side of Eq. (2) is much smaller than and can be neglected against the term $\mathrm{div}(S\,\mathrm{grad}\,c)$. This is true if molecules diffusing from a region of high towards a region of low concentration do not experience an appreciable change in the "concentration pattern" around them during their journey.

Water vapour molecules, for example, need roughly a time $t \approx l^2/(4\,D^{air}_{H_2O}) = 0.01\,\mathrm{s}$ to cover the distance $l \approx 1\,\mathrm{mm}$ from the interior of a leaf to the free atmosphere. Under normal weather conditions one can assume that atmospheric humidity needs a longer time to change appreciably (within the plant it is constant anyway). Since carbon dioxide molecules are heavier than water molecules, they move slightly slower in air than water vapour molecules, they need for the same distance $t \approx l^2/(4\,D^{air}_{CO_2}) = 0.017\,\mathrm{s}$. Atmospheric CO_2-content is practically constant during this time-span, and also the CO_2-concentration at the assimilating sites.

Appendix B. Temperature dependencies

B.1. Assimilation parameters

Bernacchi et al. (2003) give the following temperature dependencies:

$$\begin{aligned}
J_{max} &= J_{max,25\,^\circ C} \times e^{(17.57-(5236.760760/T))} \times \mu\mathrm{mol/m^2/s}\\
K &= k_{25\,^\circ C} \times K_c(1 + p_o/K_o)\\
K_c &= e^{(38.05-(9553.420009/T))} \times \mu\mathrm{mol/mol}\\
K_o &= e^{(20.30-(4375.593855/T))} \times \mathrm{mmol/mol}\\
p_o &= 210\,\mathrm{mmol/mol}\\
R_d &= R_{d,25\,^\circ C} \times e^{(18.72-(5579.543675/T))} \times \mu\mathrm{mol/m^2/s}\\
V_{max} &= V_{max,25\,^\circ C} \times e^{(26.35-(7857.546634/T))} \times \mu\mathrm{mol/m^2/s}\\
\Gamma &= \gamma_{25\,^\circ C} \times e^{(19.02-(4549.992181/T))} \times \mu\mathrm{mol/mol}\\
\Theta_{PSII} &= 0.76 + 0.018\,T - 3.7 \times 10^{-4} T^2\\
\Phi_{PSII,max} &= 0.352 + 0.022\,T - 3.4 \times 10^{-4} T^2
\end{aligned} \tag{B.1}$$

T is measured in Kelvin. The factors $V_{max,25\,^\circ C}$, $R_{d,25\,^\circ C}$, $J_{max,25\,^\circ C}$, $k_{25\,^\circ C}$ and $\gamma_{25\,^\circ C}$ which are part of the expressions V_{max}, R_d, J_{max}, K and Γ are required. (The introduction of $k_{25\,^\circ C}$ and $\gamma_{25\,^\circ C}$ represents a slight extension of the formulas of Bernacchi et al. (2003). The exact version of their formulas is recovered by setting $k_{25\,^\circ C} = 1$ and $\gamma_{25\,^\circ C} = 1$.)

B.2. Coefficients of diffusion

Nobel (1999) gives the following approximations for the temperature dependence of the coefficients of diffusion. They are (at least) valid in the range $T = 273.15 \ldots 313.15\,\mathrm{K}$ (resp. $0 \ldots 40\,^{\circ}\mathrm{C}$).

$$D_{CO_2} = \left(\frac{T}{273.15}\right)^{1.8} \times 1.33 \times 10^{-5}\ \frac{\mathrm{m}^2}{\mathrm{s}} \tag{B.2}$$

$$D_{H_2O} = \left(\frac{T}{273.15}\right)^{1.8} \times 2.13 \times 10^{-5}\ \frac{\mathrm{m}^2}{\mathrm{s}} \tag{B.3}$$

B.3. Saturation value of water vapour

The Clausius–Clapeyron equation provides an approximate (but for our purposes sufficiently correct) expression for $w_{sat}(T)$ (see Reif, 1974; Nobel, 1999)

$$w_{sat} \coloneqq \frac{u}{T}\exp\left(-\frac{v}{T}\right) \tag{B.4}$$

with $u = 2.035 \times 10^{10}\,\mathrm{mol/m^3}$ and $v = 5306$ (T in K).

Appendix C. Relation between λ and hydraulic properties of soil and plant water conduits

In order to express λ in terms of quantities characterising the hydraulic properties of: (i) the soil on which the tree grows and (ii) the tree's water transport system between roots and leaves we proceed as follows.

Since photosynthesis consumes—compared to transpiration—only a small fraction of the water flux $j^{sl}_{H_2O}$ between soil and leaves we may conclude

$$-j^{sl}_{H_2O} = E = g(\lambda)a(w_{sat} - w_a) \tag{C.1}$$

where the right-hand side repeats Eq. (21) and $g(\lambda)$ represents expression (34). (The minus sign appears because we count fluxes going out of the leaves as negative.)

On the other hand (Katul et al., 2003), $j^{sl}_{H_2O}$ is related to the water potentials in soil (Ψ_s) and leaves (Ψ_l) and to the hydraulic resistances of the conduits between soil and roots (r_{sr}) and roots and leaves (r_{rl}) by

$$j^{sl}_{H_2O} = \frac{\Psi_s - \Psi_l}{r_{sr} + r_{rl}} \tag{C.2}$$

In unsaturated soils, r_{sr} and Ψ_s can be estimated from root and soil parameters (Clapp and Hornberger, 1978):

$$r_{sr}(\theta) = \frac{\pi L_d}{K(\theta)\sqrt{R_{AI}}} \tag{C.3}$$

$$K(\theta) = K_{sat}\left(\frac{\theta}{\theta_{sat}}\right)^{2b+3} \tag{C.4}$$

$$\Psi_s(\theta) = \Psi_{sat}\left(\frac{\theta}{\theta_{sat}}\right)^{-b} \tag{C.5}$$

L_d and R_{AI} denote the root-zone depth and the root area index, θ the soil moisture content and $b > 0$ is an empirical parameter depending on soil texture. θ_{sat} denotes the value of θ if the soil is saturated with water and K_{sat} and Ψ_{sat} are the values of the soil conductance $K(\theta)$ and of the soil water potential $\Psi_s(\theta)$ at $\theta = \theta_{sat}$.

Elimination of $j^{sl}_{H_2O}$ from (C.1) and (C.2) leads to

$$g(\lambda) = \frac{\Psi_l - \Psi_s(\theta)}{a(w_{sat} - w_a)(r_{sr}(\theta) + r_{rl})} \tag{C.6}$$

Results of Tyree and Sperry (1988) suggest that the water potential within the leaves approaches the critical value Ψ_l^{crit} at which cavitation commences when transpiration is at its diurnal maximum. Maximum transpiration implies maximum conductance $g_{max}(\lambda)$ between leaves and atmosphere. Hence, at maximum transpiration expression (C.6) becomes

$$g_{max}(\lambda) = \frac{\Psi_l^{crit} - \Psi_s(\theta)}{a(\widehat{w}_{sat} - \widehat{w}_a)(r_{sr}(\theta) + r_{rl})} \tag{C.7}$$

A hat above a quantity means that this quantity should be evaluated at the temperature and/or atmospheric humidity corresponding to g_{max} (see Figs. 5 and 4).

Equating (C.7) and (34) results in a quadratic equation for λ. One of its solutions represents an unphysical artefact. The meaningful solution reads as

$$\lambda = \frac{1}{2a(\widehat{w}_{sat} - \widehat{w}_a)}\left(\widehat{C}_a + \widehat{K} - \frac{Z}{N}\right) \tag{C.8}$$

where

$$Z \coloneqq (\widehat{C}_a + \widehat{K})\left[\frac{(\widehat{C}_a + \widehat{K})(\Psi_l^{crit} - \Psi_s(\theta))}{a(\widehat{w}_{sat} - \widehat{w}_a)(r_{sr}(\theta) + r_{rl})} - (\widehat{q} - \widehat{R}_d)\right] + 2\,\widehat{q}(\widehat{K} + \widehat{\Gamma})$$

$$N \coloneqq \sqrt{\left[\frac{(\widehat{C}_a + \widehat{K})(\Psi_l^{crit} - \Psi_s(\theta))}{a(\widehat{w}_{sat} - \widehat{w}_a)(r_{sr}(\theta) + r_{rl})} - (\widehat{q} - \widehat{R}_d)\right]^2 + 4\,\widehat{q}(\widehat{K} + \widehat{\Gamma})\frac{(\Psi_l^{crit} - \Psi_s(\theta))}{a(\widehat{w}_{sat} - \widehat{w}_a)(r_{sr}(\theta) + r_{rl})}}$$

and $r_{sr}(\theta)$ and $\Psi_s(\theta)$ are as given in (C.3) and (C.5).

Fig. 15 shows the result of applying expression (C.8) to a *Ginkgo biloba* growing on clay loam and on sand (see also Table 5). The shape of both $\lambda(\theta)$-curves corroborates the interpretation of the Lagrangian multiplier λ as indicating the "cost of water": (i) an increase in soil moisture content entails a decrease in λ, (ii) the variation of λ with θ is confined to the θ-interval between the soil moisture contents related to the permanent wilting point (θ_{PWP}) and the field capacity (θ_{FC}). $\lambda(\theta)$ is practically constant within the intervals $0 < \theta < \theta_{PWP}$ and $\theta_{FC} < \theta < \theta_{sat}$ (θ_{sat} represents soil saturation).

Appendix D. Expansion of assimilation rate A and transpiration rate E for small values of λ

Expanding expression (35) for A in a series with respect to $\lambda \ll 1$ we find the following structure:

$$A = a_0 + a_1\sqrt{\lambda} + a_3\sqrt{\lambda}^3 + a_5\sqrt{\lambda}^5 + \cdots \tag{D.1}$$

where the a_k are functions of the parameters in expression (35) (apart from λ).

Eq. (21) expresses the optimum transpiration rate E as a multiple of g (see expression (34)) according to $E = ag(w_{sat} - w_a)$. Expansion in a series with respect to $\lambda \ll 1$ results in

$$E = e_{-1}\frac{1}{\sqrt{\lambda}} + e_0 + e_1\sqrt{\lambda} + e_3\sqrt{\lambda}^3 + e_5\sqrt{\lambda}^5 + \cdots \tag{D.2}$$

The e_k are functions of the parameters in expression (34), they do not depend on λ.

Appendix E. Relationship between g and v

The function $g(C_a)$ (see expression (34) and Fig. 9) is characterised by the following features (in what follows, a prime $'$ denotes differentiation with respect to C_a): (i) a zero at $C_0 > 0$ (i.e. $g(C_0) = 0$), (ii) a maximum (i.e. $g'(C_m) = 0$) at $C_m > C_0$, (iii) an asymptotic value $\lim_{C_a \to \infty} g(C_a) = 0$, (iv) a positive derivative (i.e. $g'(C_a) > 0$) within the interval $C_0 < C_a < C_m$, (v) a negative derivative

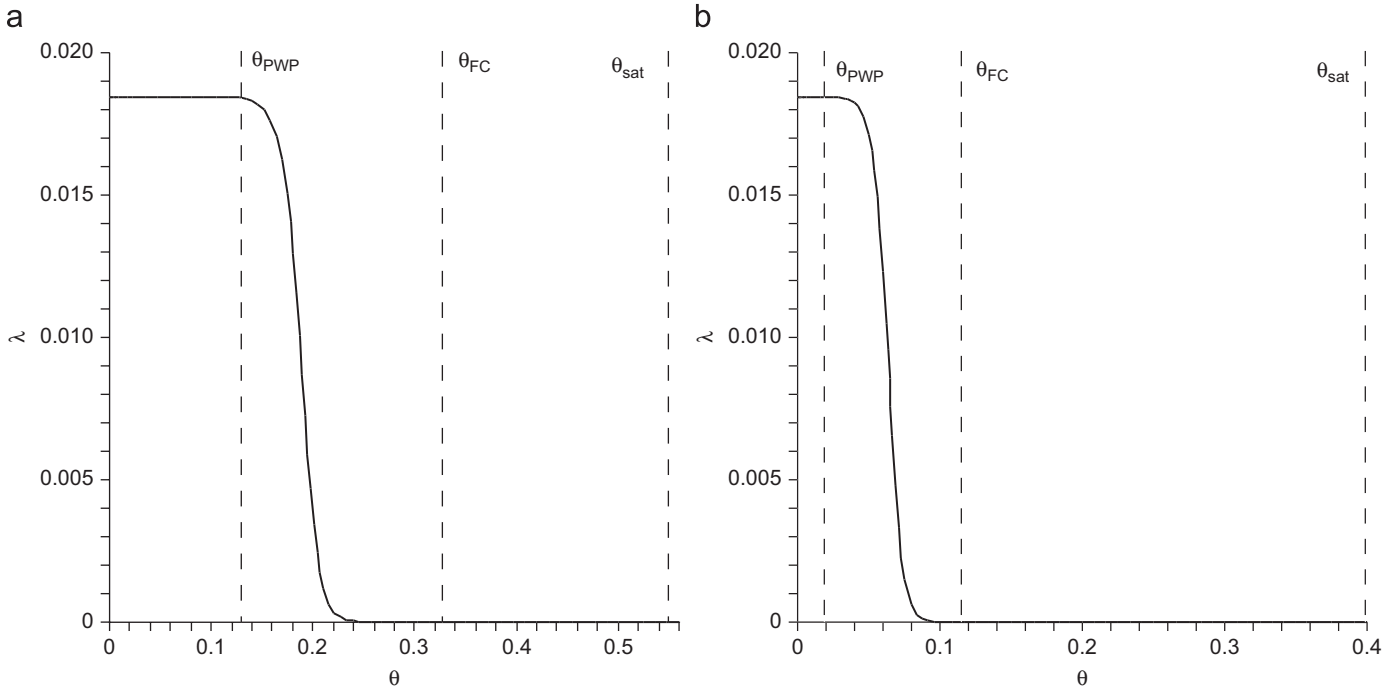

Fig. 15. Dependence of the Lagrangian multiplier λ ("cost of water") on the soil moisture content θ according to expression (C.8). Parameters used are as in Table 5. *Left*: $\lambda(\theta)$-curve of *Ginkgo biloba* growing on clay loam. *Right*: $\lambda(\theta)$-curve of *Ginkgo biloba* growing on sand. Vertical broken lines indicate soil moisture contents related to the permanent wilting point (θ_{PWP}), field capacity (θ_{FC}) and soil saturation (θ_{sat}): (a) clay loam and (b) sand.

Table 5
Hydraulic and ecophysiological parameters used in Fig. 15 (*Ginkgo biloba* growing on clay loam and on sand)

Symbol	Unit	Value for clay loam	Value for sand	Source/Remarks
Soil				
K_{sat}	m/s	3.39×10^{-6}	19.4×10^{-6}	Katul et al. (2003)
Ψ_{sat}	Pa	−1147	−637	Katul et al. (2003)
b	–	4.95	2.56	Katul et al. (2003)
θ_{sat}	–	0.55	0.40	Katul et al. (2003)
Root				
L_d	m	0.3	1.0	Katul et al. (2003)
R_{AI}	m^2/m^2	5.46	14.19	Katul et al. (2003)
Plant				
L_{AI}	m^2/m^2	3.8	1.8	Katul et al. (2003)
Ψ_l^{crit}	MPa	−1.8	−1.8	Estimate
r_{rl}	Pa m^2 s/mol	1538	934	Katul et al. (2003)
w_a	mmol/mol	637	637	See Table 2
T	°C	19.07	19.07	See Table 2

(i.e. $g'(C_a)<0$) within the interval $C_a>C_m$. (Values of $g(C_a)$ for $C_a<C_0$ are not meaningful for us.)

We show now that the function

$$v(C_a)=\frac{1}{a_{st}}\frac{\left[d_{st}^{geom}+\sqrt{\frac{a_{st}}{\pi}}\right]g(C_a)}{\left\{D_{CO_2}-\left[d_{bl}+d_{as}\frac{\tau_{as}^2}{n_{as}}\right]g(C_a)\right\}} \tag{E.1}$$

$v(C_a)$ (as given in (36)) inherits the properties (i) through (v) from $g(C_a)$. Differentiating (E.1) with respect to C_a we find

$$v'(C_a)=\frac{1}{a_{st}}\frac{D_{CO_2}\left[d_{st}^{geom}+\sqrt{\frac{a_{st}}{\pi}}\right]}{\left\{D_{CO_2}-\left[d_{bl}+d_{as}\frac{\tau_{as}^2}{n_{as}}\right]g(C_a)\right\}^2}g'(C_a) \tag{E.2}$$

Provided that the braces in the denominators of (E.1) and (E.2) are strictly positive (which will be shown below), it is obvious that (E.1) implies $v(C_0)=0$ and $\lim_{C_a\to\infty}v(C_a)=0$. Since D_{CO_2} and the anatomical quantities are positive we may conclude from (E.2) $v'(C_m)=0$, $v'(C_a)>0$ for $C_0<C_a<C_m$, and $v'(C_a)<0$ for $C_a>C_m$.

In order to show that the expression $\{D_{CO_2}-[d_{bl}+d_{as}(\tau_{as}^2/n_{as})]g(C_a)\}$ is strictly positive for $C_a>C_0$ we start from expression $n_{st}=a_{st}\,v$ (see (13)) for the porosity of the stomatal layer. $a_{st}\,v=1$ is—irrespective of the value of C_a—certainly an upper limit for the stomatal density even if this upper limit is not realistic: it implies that the leaf surface is completely covered with stomatal openings. From (19) we conclude that the conductance corresponding to $a_{st}\,v=1$ reads as

$$g_{ul}=\frac{D_{CO_2}}{d_{bl}+d_{as}\frac{\tau_{as}^2}{n_{as}}+d_{st}} \tag{E.3}$$

Then we find for the denominators of (E.1) and (E.2)

$$\begin{aligned}\left\{D_{CO_2}-\left[d_{bl}+d_{as}\frac{\tau_{as}^2}{n_{as}}\right]g(C_a)\right\}&>D_{CO_2}-\left[d_{bl}+d_{as}\frac{\tau_{as}^2}{n_{as}}\right]g_{ul}\\&=D_{CO_2}-\frac{\left[d_{bl}+d_{as}\frac{\tau_{as}^2}{n_{as}}\right]D_{CO_2}}{d_{bl}+d_{as}\frac{\tau_{as}^2}{n_{as}}+d_{st}}\\&=\frac{D_{CO_2}\,d_{st}}{d_{bl}+d_{as}\frac{\tau_{as}^2}{n_{as}}+d_{st}}\geqslant 0\end{aligned} \tag{E.4}$$

where the first step uses the finding that g_{ul} represents an upper limit of $g(C_a)$) (i.e. $g_{ul}>g(C_a)$). The second step exploits (E.3). Additionally, we rely on all anatomical quantities being positive.

This completes the proof that $v(C_a)$ shares the properties (i) through (v) (and thus its shape) with $g(C_a)$.

References

Aalto, T., Juurola, E., 2002. A three-dimensional model of CO_2 transport in air-spaces and mesophyll cells of a silver birch leaf. Plant Cell Environ. 25, 1399–1409.

Ainsworth, E.A., Long, S.P., 2005. What have we learned from fifteen years of free air carbon dioxide enrichment (FACE)? A meta-analytic review of the responses of photosynthesis canopy properties and plant production to rising CO_2. New Phytol. 165, 351–372.

Ainsworth, E.A., Rogers, A., 2007. The response of photosynthesis and stomatal conductance to rising [CO_2]: mechanisms and environmental interactions. Plant Cell Environ. 30, 258–270.

Arfken, G., 1970. Mathematical Methods for Physicists. Academic Press, New York.

Aris, R., 1975. The Mathematical Theory of Diffusion and Reaction in Permeable Catalysts. The Theory of the Steady State. Oxford University Press, London.

Beerling, D.J., 2002. Low atmospheric CO_2 levels during the Permo-Carboniferous glaciation inferred from fossil lycopsids. PNAS 99, 12567–12571.

Beerling, D.J., Kelly, C.K., 1997. Stomatal density responses of temperate woodland plants over the past seven decades of CO_2 increase: a comparison of Salisbury (1927) with contemporary data. Am. J. Bot. 84, 1572–1583.

Beerling, D.J., Royer, D.L., 2002. Reading a CO_2 signal from fossil stomata. New Phytol. 153, 387–397.

Beerling, D.J., Birks, H.H., Woodwarf, F.I., 1995. Rapid late-glacial atmospheric CO_2, changes reconstructed from the stomatal density record of fossil leaves. J. Quat. Sci. 10, 379–384.

Beerling, D.J., McElwain, J.C., Osborne, C.P., 1998. Stomatal responses of the 'living fossil' *Ginkgo biloba* L. to changes in atmospheric CO_2 concentrations. J. Exp. Bot. 49, 1603–1607.

Bernacchi, C.J., Pimentel, C., Long, S.P., 2003. *In vivo* temperature response functions of parameters required to model RuBP-limited photosynthesis. Plant Cell Environ. 26, 1419–1430.

Berner, R.A., Kothvala, Z., 2001. GEOCARBIII: a revised model of atmospheric CO_2 over Phanerozoic time. Am. J. Sci. 301, 182–204.

Berninger, F., Mäkelä, A., Hari, P., 1996. Optimal control of gas exchange during drought: empirical evidence. Ann. Bot. 77, 469–476.

Buckley, T.N., Miller, J.M., Farquhar, G.D., 2002. The mathematics of linked optimisation for water and nitrogen use in a canopy. Silva Fenn. 36, 639–669.

Clapp, R., Hornberger, G., 1978. Empirical equations for some soil hydraulic properties. Water Resour. Res. 14, 601–604.

Copeland, E.B., 1902. The mechanism of stomata. Ann. Bot. 16, 327–364.

Cowan, I.R., 1977. Stomatal behaviour and environment. Adv. Bot. Res. 4, 117–228.

Cowan, I.R., Farquhar, G.D., 1977. Stomatal function in relation to leaf metabolism and environment. Symp. Soc. Exp. Biol. 31, 471–505.

Denk, T., Velitzelos, D., 2002. First evidence of epidermal structures of Ginkgo from the Mediterranean Tertiary. Rev. Palaeobot. Palynol. 120, 1–15.

Farquhar, G.D., von Caemmerer, S., Berry, J.A., 1980. A biochemical model of photosynthetic CO_2 assimilation in leaves of C_3 species. Planta 149, 78–90.

Farquhar, G.D., von Caemmerer, S., Berry, J.A., 2001. Models of photosynthesis. Plant Physiol. 125, 42–45.

Farquhar, G.D., Buckley, T.N., Miller, J.M., 2002. Optimal stomatal control in relation to leaf area and nitrogen content. Silva Fenn. 36, 625–637.

Garcia-Amorena, I., Wagner, F., van Hoof, T.B., Gomez Manzaneque, F.G., 2006. Stomatal responses in deciduous oaks from southern Europe to the anthropogenic atmospheric CO_2 increase; refining the stomatal-based CO_2 proxy. Rev. Palaeobot. Palynol. 141, 303–312.

Hari, P., Mäkelä, A., Korpilahti, E., Holmberg, M., 1986. Optimal control of gas exchange. Tree Physiol. 2, 169–175.

Hovenden, M.J., Schimanski, L.J., 2000. Genotypic differences in growth and stomatal morphology of Southern Beech, *Nothofagus cunninghamii*, exposed to depleted CO_2 concentrations. Aust. J. Plant Physiol. 27, 281–287.

Katul, G.G., Ellsworth, D.S., Lai, C.-T., 2000. Modelling assimilation and intercellular CO_2 from measured conductance: a synthesis of approaches. Plant Cell Environ. 23, 1313–1328.

Katul, G.G., Leuning, R., Oren, R., 2003. Relationship between plant hydraulic and biochemical properties derived from a steady-state coupled water and carbon transport model. Plant Cell Environ. 26, 339–350.

Kouwenberg, L.L., McElwain, J.C., Kürschner, W., Wagner, F., Beerling, D.J., Mayle, F.E., Visscher, H., 2003. Stomatal frequency adjustment of four conifer species to historical changes in atmospheric CO_2. Am. J. Bot. 90, 610–619.

Kürschner, W.M., 1996. Leaf stomata as biosensors of palaeoatmospheric CO_2 levels. Laboratory of Palaeobotany and Palynology. Utrecht University, Utrecht.

Kürschner, W.M., Kvacek, Z. Dilcher, D.L., 2008. The impact of Miocene atmospheric carbondioxide fluctuations on climate and the evolution of terrestrial ecosystems. PNAS 105, 449–453.

Kürschner, W.M., van der Burgh, J., Visscher, H., Dilcher, D.L., 1996. Oak leaves as biosensors of late Neogene and early Pleistocene palaeoatmospheric CO_2 concentrations. Mar. Micropalaeontol. 27, 299–312.

Kürschner, W.M., Stulen, I., Wagner, F., CKuiper, P.J., 1998. Comparison of palaeobotanical observations with experimental data on the leaf anatomy of Durmast oak [*Quercus petraea* (Fagaceae)] in response to environmental change. Ann. Bot. 81, 657–664.

Lake, J.A., Quick, W.P., Beerling, D.J., Woodward, F.I., 2001. Plant development—signals from mature to new leaves. Nature 411, 154.

Lake, J.A., Woodward, F.I., PQuick, W., 2002. Long-distance CO_2 signalling in plants. J. Exp. Bot. 53, 183–193.

Lawson, T., Craigon, J., Black, C.R., Colls, J.J., Landon, G., Weyers, J.D.B., 2002. Impact of elevated CO_2 and O_3 on gas exchange parameters and epidermal characteristics in potato (*Solanum tuberosum* L.). J. Exp. Bot. 53, 737–746.

Long, S.P., Ainsworth, E.A., Rogers, A., Ort, D.R., 2004. Rising atmospheric carbon dioxide: plants FACE the future. Annu. Rev. Plant Biol. 55, 591–628.

Mäkelä, A., Berninger, F., Hari, P., 1996. Optimal control of gas exchange during drought: theoretical analysis. Ann. Bot. 77, 461–467.

McElwain, J.C., Mayle, F.E., Beerling, D.J., 2002. Stomatal evidence for a decline in atmospheric CO_2 concentrations during the Younger Dryas stadial: a comparison with Antarctic ice core records. Quat. Sci. 17, 21–29.

Medlyn, B.E., Badeck, F.W., De Pury, D.G.G., Barton, C.V.M., Broadmeadow, M., Ceulemans, R., De Angelis, P., Forstreuter, M., Jach, M.E., Kellomäki, S., Laitat, E., Marek, M., Philippot, S., Rey, A., Strassemeyer, J., Laitinen, K., Liozon, R., Portier, B., Roberntz, P., Wang, K., Jarvis, PG., 1999. Effects of elevated [CO_2] on photosynthesis in European forest species: a meta-analysis of model parameters. Plant Cell Environ. 22, 1475–1495.

Medlyn, B.E., Barton, C.V.M., Broadmedow, M.S.J., Ceulemans, R., De Angelis, P., Forstreuter, M., Freeman, M., Jackson, S.B., Kellomäki, S., Laitat, E., Rey, A., Roberntz, P., Sigurdsson, B.D., Strassemeyer, J., Wang, K., Curtis, P.S., Jarvis, P.G., 2001. Stomatal conductance of forest species after long-term exposure to elevated CO_2 concentration: a synthesis. New Phytol. 149, 247–264.

Napp-Zinn, K., 1966. Anatomie des Blattes. I: Blattanatomie der Gymnospermen. Borntraeger, Berlin.

Nobel, P.S., 1999. Physicochemical and Environmental Plant Physiology, second ed. Academic Press, New York.

Overdieck, D., Strassemeyer, J., 2005. Gas exchange of *Ginkgo biloba* leaves at different CO_2 concentration levels. Flora 200, 159–167.

Pagani, M., Zachos, J.C., Freeman, K.H., Tipple, B., Bohaty, S., 2005. Marked decline in atmospheric carbon dioxide concentrations during the paleogene. Science 309, 600–603.

Parkhurst, D.F., 1994. Diffusion of CO_2 and other gases inside leaves. Phytology 126, 449–479.

Parkhurst, D.F., Mott, K.A., 1990. Intercellular diffusion limits to CO_2 uptake in leaves. Plant Physiol. 94, 1024–1032.

Penuelas, J., Matamala, R., 1990. Changes in N and S leaf content, stomatal density and specific leaf area in 14 plant species during the last three centuries. J. Exp. Bot. 41, 1119–1124.

Poole, I., Kürschner, W.M., 1999. Stomatal Density and Index: The Practice. The Geological Society, London.

Prentice, I., Farquhar, G., Fasham, M., Goulden, M., Heinmann, M., et al., 2001. The carbon cycle and atmospheric carbon dioxide. In: Houghton, J.T., Ding, Y., Griggs, D.J., Noguer, M., van der Linden, P.J., et al. (Eds.), Climate Change 2001: The Scientific Basis. Contributions of Working Group I to the Third Assessment Report of the Intergovernmental Panel on Climate Change. Cambridge University Press, Cambridge, UK, pp. 183–238.

Reich, P.B., Hungate, B.A., Luo, Y., 2006. Carbon–nitrogen interactions in terrestrial ecosystems in response to rising atmospheric carbon dioxide. Annu. Rev. Ecol. Evol. Systematics 37, 611–636.

Reid, C.D., Maherali, H., Johnson, H.B., Smith, S.D., Wullschleger, S.D., Jackson, R.B, 2003. On the relationship between stomatal characters and atmospheric CO_2. Geophys. Res. Lett. 30, Article no. 1983.

Reif, F., 1974. Fundamentals of Statistical and Thermal Physics. McGraw-Hill, New York.

Royer, D.L., 2001. Stomatal density and stomatal index as indicators of palaeoatmospheric CO_2 concentration. Rev. Palaeobot. Palynol. 114, 1–28.

Royer, D.L., Wing, S.L., Beerling, D.J., Jolley, D.W., Koch, P.L., Hickey, L.J., Berner, R.A., 2001. Paleobotanical evidence for near present-day levels of atmospheric CO_2 during part of the Tertiary. Science 292, 2310–2313.

Senatsverwaltung für Stadtentwicklung Berlin, 1993. Digitaler Umweltatlas Berlin (Ausgabe 1993), 04.04 Temperatur- und Feuchteverhältnisse in mäßig austauscharmen Strahlungsnächten, ⟨http://www.stadtentwicklung.berlin.de/umwelt/umweltatlas/din_404.htm⟩.

Stitt, M., Krapp, A., 1999. The interaction between elevated carbon dioxide and nitrogen nutrition: the physiological and molecular background. Plant Cell Environ. 22, 581–621.

Sun, B., Dilcher, D.L., Beerling, D.J., Zhang, C., Yan, D., Kowalski, E., 2003. Variation in *Ginkgo biloba* L. leaf characters across a climatic gradient in China. PNAS 100, 7141–7146.

Teng, N., Wang, J., Chen, T., Wu, X., Wang, Y., Lin, J., 2006. Elevated CO_2 induces physiological, biochemical and structural changes in leaves of *Arabidopsis thaliana*. New Phytol. 172, 92–103.

Tricker, P.J., Trewin, H., Kull, O., Clarkson, G.J.J., Eensalu, E., Tallis, M.J., Colella, A., Doncaster, C.P., Sabatti, M., Taylor, G., 2005. Stomatal conductance and not

stomatal density determines the long-term reduction in leaf transpiration of poplar in elevated CO_2. Oecologia 143, 652–660.
Tyree, M.T., Sperry, J.S., 1988. Do woody plants operate near the point of catastrophic xylem dysfunction caused by dynamic water stress? Plant Physiol. 88, 574–580.
van de Water, P.K., Leavitt, S.W., Betancourt, J.L., 1994. Trends in stomatal density and $^{13}C/^{12}C$ ratios of *Pinus flexilis* during last glacial–interglacial cycle. Science 264, 239–242.
Woodward, F.I., 1987. Stomatal numbers are sensitive to increases in CO_2 concentration from pre-industrial levels. Nature 327, 617–618.
Woodward, F.I., Bazzazz, F.A., 1988. The responses of stomatal density to CO_2 partial pressure. J. Exp. Bot. 39, 1771–1781.
Woodward, F.I., Lake, J.A., PQuick, W., 2002. Stomatal development and CO_2: ecological consequences. New Phytol. 153, 477–484.
Wynn, J.G., 2003. Towards a physically based model of CO_2-induced stomatal frequency response. New Phytol. 157, 394–398.